



# Effect of the $\text{SiO}_2/\text{Al}_2\text{O}_3$ Molar Ratio on the Microstructure and Properties of Clay-based Geopolymers: A Comparative Study of Kaolinite-based and Halloysite-based Geopolymers

Baifa Zhang · Ting Yu · Haozhe Guo ·  
Jiarong Chen · Yi Liu · Peng Yuan

Accepted: 16 March 2023 / Published online: 24 March 2023  
© The Author(s), under exclusive licence to The Clay Minerals Society 2023

**Abstract** As 1:1 dioctahedral clay minerals, kaolinite and halloysite have similar chemical compositions. However, halloysite often possesses a nanotubular structure and special surface reactivity compared to platy kaolinite. The objective of this current work was to determine the effect of the  $\text{SiO}_2/\text{Al}_2\text{O}_3$  ratio on the microstructure and properties of geopolymers derived from two kinds of kaolin: platy kaolinite and nanotubular halloysite. The chemical structures and compositions of the geopolymers obtained were characterized through X-ray diffraction (XRD), Fourier-transform infrared (FTIR) spectroscopy, and nuclear magnetic resonance (NMR), whereas the microstructural analysis was performed by scanning electron microscopy (SEM),

the Brunauer–Emmett–Teller (BET) method, and  $\text{N}_2$  physisorption analysis. The results indicated that calcined halloysite showed greater geopolymerization reactivity than calcined kaolinite. In addition, the mechanical properties of the clay-based geopolymers depended not only on the  $\text{SiO}_2/\text{Al}_2\text{O}_3$  ratio but also on the morphology of the clay. Crystalline zeolite A and geopolymer were produced after alkali-activation of kaolin with a  $\text{SiO}_2/\text{Al}_2\text{O}_3$  ratio of 2.5; these products possessed porous and heterogeneous microstructures having poor compressive strength. As  $\text{SiO}_2/\text{Al}_2\text{O}_3$  ratios increased to >2.5, geopolymers with compact microstructure and high compressive strength were produced after alkali-activation of kaolin. Notably, at a given condition, halloysite-based geopolymers exhibited greater early compressive strength, more compactness, and more homogeneous microstructure than kaolinite-based geopolymers. This can be attributed to the nanotubular microstructure of halloysite, which can release more Si and Al during alkali activation than platy kaolinite. These results indicated that the various morphologies and microstructures among clays have significant impact on the microstructure and compressive strength of geopolymers.

Associate Editor: Victoria Krupskaya.

B. Zhang (✉) · Y. Liu · P. Yuan  
School of Environmental Science and Engineering,  
Guangdong University of Technology, Guangzhou 510006,  
China  
e-mail: zhangbaifa@gdut.edu.cn

T. Yu · J. Chen  
CAS Key Laboratory of Mineralogy and Metallogeny/  
Guangdong Provincial Key Laboratory of Mineral Physics  
and Materials, Guangzhou Institute of Geochemistry,  
Institutions of Earth Science, Chinese Academy  
of Sciences, Guangzhou 510640, China

H. Guo  
Institute of Resource Comprehensive Utilization,  
Guangdong Academy of Sciences, Guangzhou 510650,  
China

**Keywords** Dissolution · Geopolymer · Halloysite ·  
Kaolinite ·  $\text{SiO}_2/\text{Al}_2\text{O}_3$  ratio

## Introduction

Alkali-based geopolymer is a kind of inorganic polymeric material comprising cross-linked tetrahedral

[AlO<sub>4</sub>] and [SiO<sub>4</sub>] units, having a three-dimensional network structure, where hydrated alkali metal cations (e.g. Na<sup>+</sup>, K<sup>+</sup>, etc.) are distributed throughout the network to balance the negative charges of [AlO<sub>4</sub>]<sup>-</sup> (Amran et al., 2020; Najafi et al., 2020). As a new type of cementitious material, geopolimer has been regarded as a potential alternative to ordinary Portland cement (OPC) because it not only consumes less energy and emits less CO<sub>2</sub> during manufacturing but also exhibits better properties, including greater mechanical strength, better fire resistance, and greater durability (Farhan et al., 2019; Tognonvi et al., 2020; Chen et al., 2021). Normally, alkali-based geopolimer is synthesized by the dissolution of aluminosilicates into an alkaline activator, followed by a curing process (Zhang et al., 2021). In general, raw materials, such as clays (Liew et al., 2016; Werling et al., 2022), industrial waste (Shekhovtsova et al., 2018; Zhang et al., 2022), and other aluminosilicate-rich material with sufficient reactive alumina and silica (Nana et al., 2019; Wang et al., 2022), can be used for geopolimer preparation.

Clay minerals are naturally occurring minerals found around the world which are important raw materials in various domains (Mbey et al., 2019). Kaolinite (Al<sub>2</sub>(OH)<sub>4</sub>Si<sub>2</sub>O<sub>5</sub>, Kln) is a typical 1:1 dioctahedral clay mineral, which usually has a hexagonal flake or plate-like shape. Each layer of Kln contains a silica tetrahedral sheet and an alumina octahedral sheet and these sheets are bound by sharing oxygen atoms, while adjacent sheets are bound by hydrogen bonds (Deng et al., 2017; Li et al., 2020). Kln has been applied in the stabilization of contaminated soil (Liu et al., 2020), supplementary cementitious materials (Haw et al., 2020), and ceramic preparations (Prasad et al., 1991). Kln is also widely used for geopolimer preparation and geopolimerization mechanism analysis due to its high pozzolanic activity and simple chemical composition (Lolli et al., 2018; Wang et al., 2020). Compared to other precursors, such as red mud (He et al., 2012), fly ash (Cai et al., 2020), or illite (Hu et al., 2016), geopolimer derived from alkali activation of Kln shows greater compressive strength, shorter setting time, and better thermoelectrical properties. Many factors (e.g. SiO<sub>2</sub>/Al<sub>2</sub>O<sub>3</sub> molar ratio, liquid/solid ratio, and curing conditions etc.) have been reported previously to impact on the microstructure and mechanical properties of Kln-based geopolimers (Duxson et al., 2007; Heah et al., 2012; Qian et al., 2017; Yuan et al.,

2016). Among these, the SiO<sub>2</sub>/Al<sub>2</sub>O<sub>3</sub> molar ratio is one of the most important factors in geopolimer preparation, which controls the microstructure, chemical composition, and properties of as-obtained products (Liew et al., 2016; Tian et al., 2021; Liu et al., 2022). Qian et al. (2017) found that the compressive strength of calcined Kln-based geopolimer increased from 2.1 to 31.2 MPa when the Si/Al ratio increased from 1.0 to 2.0, while it decreased to 5.5 MPa when the Si/Al ratio increased to 5.0. Khalifa et al. (2020) also concluded that during alkali-activation, geopolimer was formed when Si/Al > 1.5, and zeolite was formed when Si/Al < 1.5.

Halloysite (Al<sub>2</sub>(OH)<sub>4</sub>Si<sub>2</sub>O<sub>5</sub>·2H<sub>2</sub>O, Hly) is also a 1:1 dioctahedral clay mineral, showing some similarities in chemical composition to Kln. However, due to an additional monolayer of water molecules between the unit layers of Hly, the mismatch between the tetrahedral SiO<sub>4</sub> and octahedral AlO<sub>6</sub> sheets of adjacent layers causes the wrapping of the 1:1 aluminosilicate layers, thus forming a nanosized tubular structure (Singh, 1996; Yuan et al., 2008; Yuan, 2016). Owing to its nanotubular structure, Hly normally possesses a larger specific surface area, less chemical stability, and lower ordering degree than Kln (White et al., 2012; Yuan et al., 2015). These different features between Hly and Kln might lead to a different geopolimerization process.

In fact, many previous studies have proposed that the geopolimerization behavior is also affected significantly by the morphologies and structure of Kln. For example, through different calcination technologies, Medri et al. (2010) and Nicolas et al. (2013) prepared various morphologies of metakaolinite. They found that metakaolinite powder with rounded agglomerates was more sensitive to the geopolimerization condition and required less water during geopolimerization than lamellar ones. Hollanders et al. (2016) compared the pozzolanic activity of Klns from different regions. They found that the raw Kln with a lower degree of ordering required a lower activation temperature, which had greater pozzolanic activity and a faster pozzolanic reaction rate. Zhang et al. (2016) noted different reactivity and geopolimerization behavior between Kln and Hly. They reported that the leaching rate of Si and Al from uncalcined Longyan kaolin (containing 31 wt.% Hly and 52 wt.% Kln) in strong alkaline solution was very close to that of the Suzhou kaolin (containing 91 wt.% Kln) calcined at

700°C for 1 h. Moreover, they also found that geopolymers prepared from Longyan kaolin exhibited greater geopolymerization reactivity (e.g. faster setting, faster development of compressive strength) than that from Suzhou kaolin (Zhang et al., 2012a).

Therefore, the use of Hly as a geopolymer precursor has attracted increasing attention. Kaze et al. (2018) used Cameroon-metahalloysite for geopolymer preparation and received products with a maximum compressive strength of ~27.5 MPa. They also found that by increasing the calcination temperature from 600 to 750°C, the reactive phase content of Hly increased, which shortened the setting time and improved the rheological behavior of geopolymer pastes (Kaze et al., 2020a). Zhang et al. (2020b) studied the effects of calcination temperatures on the microstructure and compressive strength of Hly-based geopolymer and found that when calcination temperature reached 750°C, the Hly-based geopolymer exhibited a compact microstructure and the greatest compressive strength. All these results indicated that Hly is a promising precursor for geopolymer preparation.

The results above also demonstrated that the geopolymerization process of Hly differs from that of Kln (Izadifar et al., 2020; Zhang et al., 2020c). Although a recent study from Tchakouté et al. (2020) compared the microstructural and mechanical properties of Kln-based geopolymers with Hly-based ones, the Hly used in that study was spherical, while the dominant morphology of naturally occurring Hly is tubular (Yuan et al., 2015). In addition, both Kln and Hly samples contain many impurities. This may limit the widespread applicability of conclusions from any specific study. Moreover, the studies of Hly-based geopolymer are far less reported than those for other precursors (e.g. Kln, illite, and fly ash, etc.). The effects of the SiO<sub>2</sub>/Al<sub>2</sub>O<sub>3</sub> ratio on the microstructure and mechanical properties of Hly-based geopolymer remain unknown even though it can control the phase formation.

The objective of the current study was to compare the effect of the SiO<sub>2</sub>/Al<sub>2</sub>O<sub>3</sub> ratio on the microstructure and mechanical properties of platy Kln-based and nanotubular Hly-based geopolymers to enable a further understanding of the effect of morphology of 1:1 dioctahedral clay minerals on their geopolymerization process and on the geopolymers obtained. This work will provide a better insight into the various geopolymerization behaviors between Kln and Hly as well as the properties of as-obtained geopolymers.

## Experimental

### Materials

Two kinds of precursors, i.e. platy kaolinite (Kln) and nanotubular halloysite (Hly), were used for the preparation of geopolymers by alkali activation. Kln was collected from Maoming, Guangdong, and Hly was provided by I-Minerals, Inc., Vancouver, Canada. The chemical compositions of Kln and Hly measured by X-ray fluorescence (XRF) are presented in Table 1. The Kln and Hly powders were calcined in a muffle furnace at 750°C in air for 2 h (heating/cooling rate of 5°C/min) and were denoted as Kln<sub>750°C</sub> and Hly<sub>750°C</sub>, respectively.

The alkaline activator was prepared by mixing analytical-grade NaOH pellets (purity ≥ 96%) with commercial sodium silicate (original SiO<sub>2</sub> 26.5 wt.%, Na<sub>2</sub>O 8.5 wt.%, and water 65.0 wt.%) and Milli-Q water. The solution used in leaching was 10 mol/L NaOH solution. Solutions were stored for 24 h prior to use.

### Preparation of Clay-based Geopolymers

Kln<sub>750°C</sub> or Hly<sub>750°C</sub> powders were mixed with the alkaline activator to prepare the geopolymers. The molar ratio of SiO<sub>2</sub>/Al<sub>2</sub>O<sub>3</sub> was set as 2.5, 3.0, or 3.5 while the

**Table 1** Chemical composition of Kln and Hly (wt.%)

| Clay | SiO <sub>2</sub> | Al <sub>2</sub> O <sub>3</sub> | Fe <sub>2</sub> O <sub>3</sub> | K <sub>2</sub> O | MgO  | CaO   | Na <sub>2</sub> O | TiO <sub>2</sub> | SO <sub>3</sub> | L.O.I. |
|------|------------------|--------------------------------|--------------------------------|------------------|------|-------|-------------------|------------------|-----------------|--------|
| Kln  | 47.69            | 36.48                          | 0.69                           | 0.65             | 0.11 | 0.076 | 0.069             | 0.36             | 0.26            | 13.47  |
| Hly  | 46.00            | 37.80                          | 0.72                           | 0.30             | 0.13 | 0.07  | 0.01              | 0.07             | <0.01           | 14.90  |

L.O.I.: loss on ignition

molar ratio of  $\text{Na}_2\text{O}/\text{Al}_2\text{O}_3$  was set to 1.0. However, due to the various minimum water requirements for workability of  $\text{Kln}_{750^\circ\text{C}}$  and  $\text{Hly}_{750^\circ\text{C}}$ , the molar ratio of  $\text{H}_2\text{O}/\text{Na}_2\text{O}$  was set to 10.0 and 11.5 for  $\text{Kln}_{750^\circ\text{C}}$  and  $\text{Hly}_{750^\circ\text{C}}$ , respectively. The resulting geopolymeric paste was poured into 20 mm  $\times$  20 mm  $\times$  12 mm plastic molds and covered with a thin film of polyethylene. The molded specimens were cured at 50°C for 48 h and then were further cured at 80°C for another 48 h. The hardened samples were demolded and sealed in plastic bags at ambient temperature. The products obtained were labeled  $\text{Kln}_{750^\circ\text{C}}\text{-X}$  or  $\text{Hly}_{750^\circ\text{C}}\text{-X}$ , where X represents the molar ratio of  $\text{SiO}_2/\text{Al}_2\text{O}_3$  of the raw materials. For example,  $\text{Kln}_{750^\circ\text{C}}\text{-2.5}$  is the alkali-activation product with a  $\text{SiO}_2/\text{Al}_2\text{O}_3$  molar ratio of 2.5.

### Characterization of Clay-based Geopolymers

1 g of  $\text{Kln}_{750^\circ\text{C}}$  or  $\text{Hly}_{750^\circ\text{C}}$  was mixed with 30 g of 10 mol/L NaOH solutions at  $25 \pm 2^\circ\text{C}$  in a shaker for various times. Then, after centrifugation and filtration, the leachate was separated. The concentrations of Si and Al dissolved from raw materials were determined by an iCAP 7000 Series inductively coupled plasma optical emission spectrometry instrument (Thermo Fisher Scientific Inc., Waltham, Massachusetts, USA).

The setting times of pastes prepared by mixing the  $\text{Kln}_{750^\circ\text{C}}$  or  $\text{Hly}_{750^\circ\text{C}}$  with alkaline activator were tested by a Vicat apparatus. 7- and 28-day compressive strengths of geopolymers were performed on a YAW-300D Compression Resistance Tester (Schlikör, LiXian, Zhejiang, China) with a loading rate of 500 N/s.

Thermogravimetric (TG) analyses were performed on a Netzsch STA 409PC instrument (Selb, Bayern, Germany) for  $\text{Kln}$  and  $\text{Hly}$ . Powdered samples (~10 mg) were analyzed by heating in a corundum crucible from 30 to 1000°C at a rate of 10°C/min.

The XRD patterns of clays, calcined clays, and 28-day geopolymers were collected on a Bruker D8 Advance diffractometer (Mannheim, Karlsruhe, Germany), operating at 40 kV and 40 mA using  $\text{CuK}\alpha$  radiation. The specimens were powdered finely to investigate their diffraction from 3 to  $70^\circ 2\theta$  with a scanning speed of  $3^\circ 2\theta/\text{min}$ .

The FTIR spectra of clays, calcined clays, and 28-day geopolymers were recorded on a Bruker Vertex 70 spectrometer (Mannheim, Karlsruhe, Germany). The products were mixed with 0.9 mg of sample and 90 mg of KBr and powdered finely

before the mixture was pressed into a disk for analysis. FTIR spectra of the disks were collected at 4000 to  $400\text{ cm}^{-1}$  with 64 scans, at a resolution of  $4\text{ cm}^{-1}$ .

The SEM micrographs and energy-dispersive X-ray (EDX) spectroscopy results of clays, calcined clays, and 28-day geopolymers were obtained using an SU8010 field-emission scanning electron microscope (Hitachi, Tokyo, Japan) at an accelerating voltage of 15 kV. Specimens were prepared for analysis by being anchored tightly on the surface of conducting tape, coated with a layer of platinum, and then transferred to the microscope.

Measurements of pore-size distribution and the total pore volume of 28-day geopolymers' powder were carried out by  $\text{N}_2$  physisorption analysis in a Micromeritics ASAP 2020 instrument (Micromeritics Co., Norcross, Georgia, USA) at liquid-nitrogen temperature ( $-196^\circ\text{C}$ ). Before measurements, the products were outgassed at defined temperatures for 24 h at 393 K at the degassing port. The total pore volume was obtained from  $\text{N}_2$  uptake at a relative pressure of 0.97.

Solid-state  $^{29}\text{Si}$  cross-polarization magic-angle-spinning (CP/MAS) NMR spectra and  $^{27}\text{Al}$  MAS NMR spectra of 28-day geopolymers' powder were recorded on a Bruker Avance III600 spectrometer (Mannheim, Germany). For  $^{29}\text{Si}$  CP/MAS NMR spectra, the magnetic field strength was 14.1 T with a resonance frequency of 119.2 MHz and was recorded using a contact time of 6 ms, a  $\pi/2$  pulse length of 2.3  $\mu\text{s}$ , a recycle delay of 2 s and a spinning rate of 10 kHz. For  $^{27}\text{Al}$  MAS NMR spectra, the magnetic field strength was 14.1 T with a resonance frequency of 156.4 MHz and was recorded using a small-flip angle technique with a pulse length of 0.5  $\mu\text{s}$  ( $< \pi/12$ ), a recycle delay of 1 s and a spinning rate of 14 kHz. The chemical shifts of  $^{27}\text{Al}$  and  $^{29}\text{Si}$  were given in ppm referenced to 1 mol/L  $\text{Al}(\text{NO}_3)_3$  and tetramethylsilane (TMS), respectively.

## Results and Discussion

### Characterization of $\text{Kln}$ , $\text{Hly}$ , and their Heating Products

#### *TG-DSC curve*

TG curves (Fig. 1) showed mass losses of 1.42% for  $\text{Kln}$  and 2.78% for  $\text{Hly}$  below 450°C, which were ascribed to the dehydration of  $\text{Kln}$  and  $\text{Hly}$  (loss of

physical adsorbed water and/or interlayer water). Another major mass loss occurred in the temperature range from 450 to 650°C and was associated with the dehydroxylation of Kln and Hly. Above 650°C, the mass loss continued but to a small extent up to 1000°C. The total mass losses for Kln and Hly were ~14.21% and 15.38%, respectively.

In the DSC curve, broad endothermic peaks at ~520 and 507°C for Kln and Hly, respectively, corresponded to dehydroxylation of Al–OH and Si–OH. This result indicated that, compared to Kln, the dehydroxylation of Hly starts at a lower temperature. In addition, a narrow exotherm appeared at 998°C for Kln, which should be due to the formation of spinel-like  $\gamma$ -Al<sub>2</sub>O<sub>3</sub> or an alumina-rich mullite (Okada et al., 1986; Sonuparlak et al., 2005). However, this exothermic event (990°C) of Hly during the calcination should be attributed to the formation of nanosized  $\gamma$ -Al<sub>2</sub>O<sub>3</sub> based on the <sup>29</sup>Si and <sup>27</sup>Al MAS NMR results (Smith et al., 1993). By using high-resolution TEM, Yuan (2016) also identified the formation of nanosized  $\gamma$ -Al<sub>2</sub>O<sub>3</sub> when Hly was calcined at 1000°C.

### XRD results

For Kln, most of the XRD reflections (Fig. 2) belonged to kaolinite with the strongest reflection at 12.2°2 $\theta$  (with a  $d_{001}$  of 7.25 Å). A small peak at 26.7°2 $\theta$  indicated the presence of a small amount of quartz. When calcined at 750°C, a new broad

reflection emerged at ~21.1°2 $\theta$  due to the dehydroxylation of Kln. This result indicated that the crystal structure of Kln had been destroyed and the Kln transformed into metakaolinite after heat treatment at 750°C.

The interlayer distance,  $d_{001}$ , of Hly (Fig. 2) was similar to that of Kln. This also demonstrated that the Hly used in this study is 7 Å-halloysite, from which the water monolayer was lost. The reflections belonging to halloysite disappeared and the existence of a broad reflection emerged at ~21.1°2 $\theta$  when Hly was calcined at 750°C. This also indicated that the structure of Hly was destroyed and an amorphous phase formed.

### SEM images

The SEM images (Fig. 3a,b) showed significantly different morphologies between Kln and Hly. The morphology of Kln was lamellar while that of Hly was nanotubular. When calcined at 750°C, they kept their original shapes. This result demonstrated that heating at 750°C did not change the morphology of Kln and Hly. Accordingly, their specific surface areas did not change significantly either. Determined by BET, the specific surface areas of the Kln and Kln<sub>750°C</sub> were 14.73 and 15.53 m<sup>2</sup>/g, respectively, while Hly and Hly<sub>750°C</sub> were 28.29 and 27.62 m<sup>2</sup>/g, respectively. Specifically, the specific surface area of Hly was nearly twice as large as that of Kln.

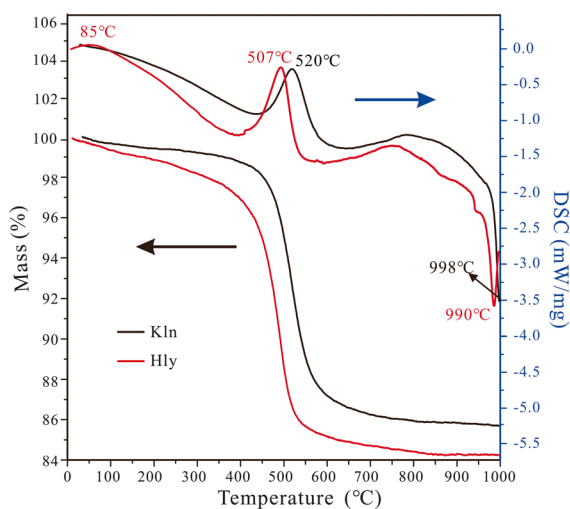


**Fig. 1** TG-DSC curves of Kln and Hly

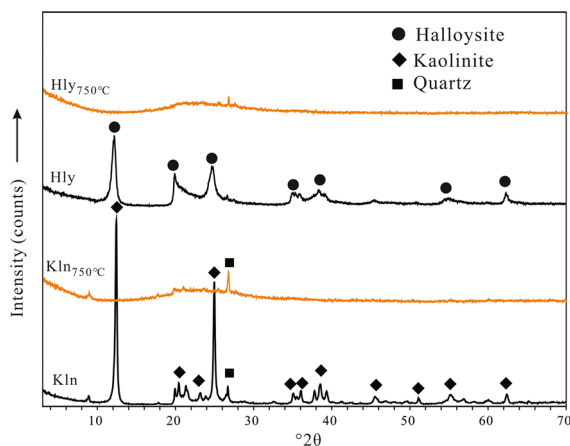


**Fig. 2** XRD patterns of Kln, Hly, and their calcination products

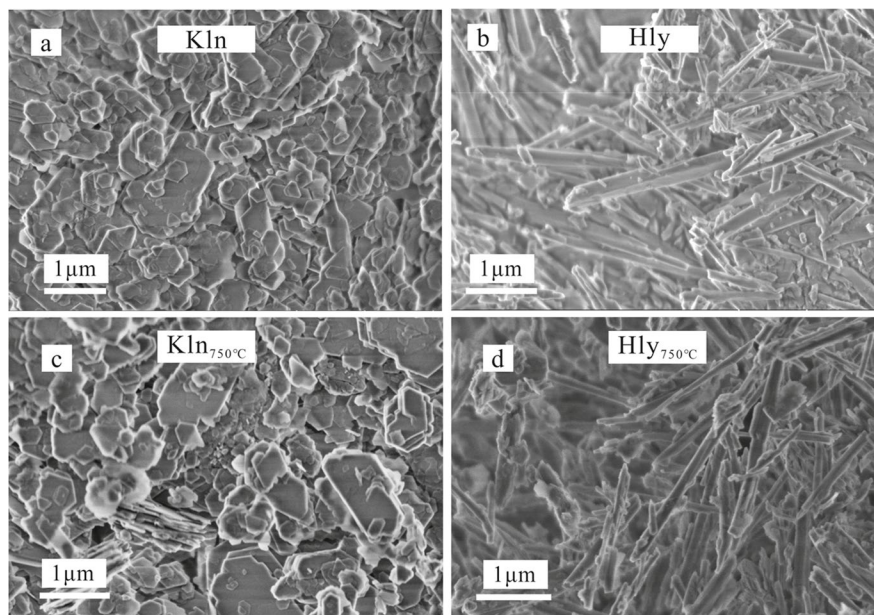


**Fig. 3** SEM images of **a** Kln, **b** Hly, **c** Kln<sub>750°C</sub> and **d** Hly<sub>750°C</sub>

### FTIR results

The spectrum of Kln (Fig. 4) exhibited four absorption bands ranging from 3700 to 3600  $\text{cm}^{-1}$ , where the peaks at 3694, 3669, and 3651  $\text{cm}^{-1}$  were attributed to the O–H stretching of inner-surface hydroxyl groups and 3620  $\text{cm}^{-1}$  was attributed to O–H stretching of inner hydroxyl groups (Madejová & Komadel, 2001). In addition, the absorption at 913  $\text{cm}^{-1}$  was also attributed to O–H vibration of inner hydroxyl groups. However, the absorption bands at 3669 and 3651  $\text{cm}^{-1}$  did not appear in the FTIR spectrum of Hly, demonstrating the lower ordered structure of Hly compared to Kln (Parker, 1969). The peak at 1103  $\text{cm}^{-1}$  was assigned to perpendicular Si–O stretching while bands at 1032 and 1009  $\text{cm}^{-1}$  were related to the in-plane Si–O stretching vibration. Moreover, the absorptions of 795, 754, 697, and 432  $\text{cm}^{-1}$  were all attributed to Si–O vibrations. The band at 539  $\text{cm}^{-1}$  was assigned to Al–O–Si deformation and 471  $\text{cm}^{-1}$  was attributed to Si–O–Si deformation (Madejová & Komadel, 2001). The peaks ranging from 1110 to 430  $\text{cm}^{-1}$  in the spectrum of Kln were similar to those of Hly, indicating the similar structures of Kln and Hly at the molecular scale.

After calcination at 750°C, the vibration corresponding to the hydroxyl group of Kln disappeared,

along with the broad band at 3433  $\text{cm}^{-1}$  which was attributed to the O–H of adsorbed water. A broad and asymmetric band centered at 1082  $\text{cm}^{-1}$  was assigned to the symmetrical stretching vibration of Si–O–Si and Si–O–Al bonds. In addition, the broad bands at 800 and 466  $\text{cm}^{-1}$  were both ascribed to the Si–O–Si stretching vibration from the amorphous silica. These results demonstrated that the structure of Kln was destroyed and amorphous SiO<sub>2</sub> was formed (Yuan et al., 2012). Similar results can also be found in the FTIR spectrum of Hly<sub>750°C</sub>.

### Dissolution behavior of Kln<sub>750°C</sub> and Hly<sub>750°C</sub>

The concentrations of Si and Al leached from the clays in NaOH solutions increased with leaching time up to 48 h and then remained nearly unchanged as leaching time increased (Table 2 and Fig. 5). The concentration of Si and Al leached from Kln<sub>750°C</sub> increased from 205.2 to 8080.5 ppm and 114.7 to 4188.7 ppm, respectively. The concentration of Si and Al leached from Hly<sub>750°C</sub> increased from 281.4 to 9253.3 ppm and 189.9 to 4274.0 ppm, respectively.

The concentrations of Si and Al leached from Hly<sub>750°C</sub> were greater than those from Kln<sub>750°C</sub> under the same leaching conditions; the leaching times

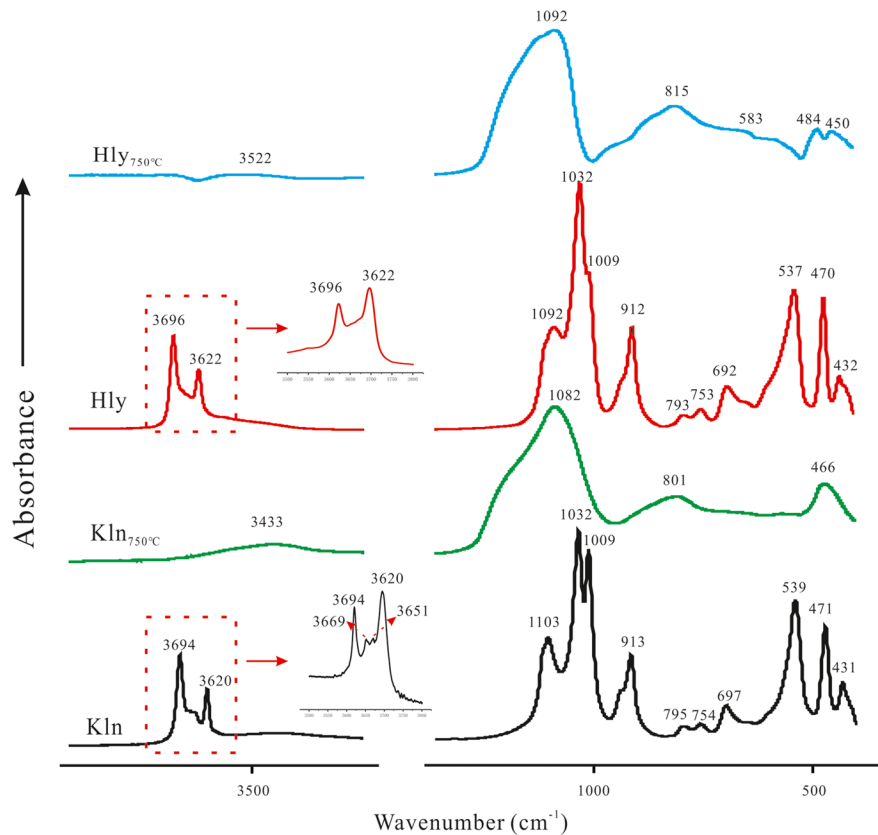


**Fig. 4** FTIR spectra of Kln, Hly, and their calcination products

from Hly<sub>750°C</sub> were shorter than from Kln<sub>750°C</sub>. This result confirmed that the pozzolanic activity of Hly is greater than that of Kln, which may favor geopolymerization. The dissolution of the aluminosilicate precursor is the first step of geopolymerization, which occurs mainly in the early stages, followed by polycondensation of oligomers. This was also evidenced by isothermal calorimetry measurement in previous studies (Sun & Vollpracht, 2017;

Zhang et al., 2012b, 2013), which found two obvious exothermic peaks 5 h after geopolymerization. Therefore, the early stage of dissolution plays an important role in the formation of geopolymeric gels. In the first 3 h, the Si and Al concentrations leached from Hly<sub>750°C</sub> were 2690.5 and 1526.7 ppm (Table 2), which was nearly three times greater than those from Kln<sub>750°C</sub>. This may lead to the improvement in the degree of geopolymerization.

**Table 2** Concentration of Al and Si leached from Kln<sub>750°C</sub> and Hly<sub>750°C</sub> in NaOH solutions

| Sample               | element  | Time (h) |        |        |        |        |        |        |        |
|----------------------|----------|----------|--------|--------|--------|--------|--------|--------|--------|
|                      |          | 0.5      | 1.0    | 2.0    | 3.0    | 5.0    | 10.0   | 48.0   | 120.0  |
| Kln <sub>750°C</sub> | Si (ppm) | 205.2    | 706.8  | 828.7  | 876.7  | 1915.3 | 5581.1 | 8080.5 | 7985.8 |
|                      | Al (ppm) | 114.7    | 417.1  | 464.1  | 484.4  | 1044.2 | 2818.0 | 3057.2 | 4188.7 |
| Hly <sub>750°C</sub> | Si (ppm) | 281.4    | 1146.3 | 2222.9 | 2690.5 | 3236.2 | 5933.7 | 9253.3 | 8896.5 |
|                      | Al (ppm) | 189.9    | 686.5  | 1283.0 | 1526.7 | 1827.3 | 3081.2 | 3137.5 | 4274.5 |

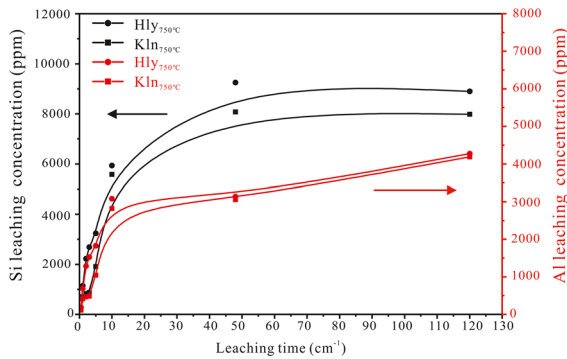


**Fig. 5** Concentrations of Si and Al dissolved from clays in NaOH solution

## Properties of Clay-based Geopolymers

### Setting Time

The setting times shown in Fig. 6 illustrated that as the  $\text{SiO}_2/\text{Al}_2\text{O}_3$  ratio increased, the initial setting time increased from 93 to 212 min and final setting time was increased from 221 to 324 min for  $\text{Kln}_{750^\circ\text{C}}$ -based geopolymeric pastes; and the initial setting time was increased from 52 to 146 min and final setting time was increased from 198 to 263 min for  $\text{Hly}_{750^\circ\text{C}}$ -based geopolymers. The alkalinity of the solution decreased gradually with the increase in the  $\text{SiO}_2/\text{Al}_2\text{O}_3$  ratio, which reduced the dissolution degree of Si and Al from precursors and thus prolonged the setting time. This was also evidenced by Zhang et al. (2013), who

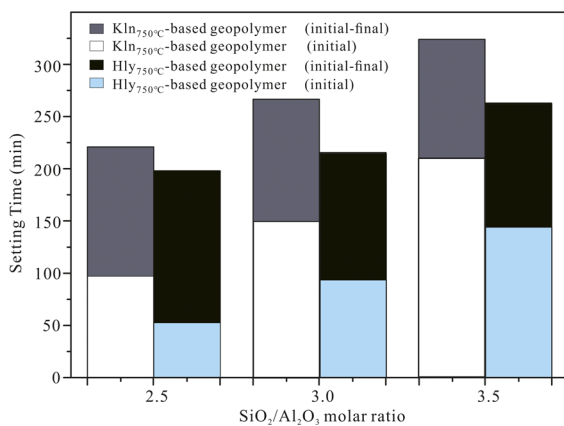


**Fig. 6** Initial and final setting time of clay-based geopolymeric pastes

reported that the greater the alkali concentration, the more rapid the geopolymerization.

As was observed, the initial and final setting times were longer for  $\text{Kln}$ -based geopolymer than  $\text{Hly}$ -based geopolymer at a given  $\text{SiO}_2/\text{Al}_2\text{O}_3$  ratio. This may be due to the fact that the greater and faster dissolution of Si and Al from  $\text{Hly}_{750^\circ\text{C}}$  than from  $\text{Kln}_{750^\circ\text{C}}$  resulted in the faster polycondensation of oligomers when mixing the clay and activator. Thus, the geopolymeric paste was hardened more quickly for alkali-activated  $\text{Hly}_{750^\circ\text{C}}$  than  $\text{Kln}_{750^\circ\text{C}}$  (Zhang et al., 2012a).

### Compressive Strength of Clay-based Geopolymers

Clay-based geopolymers with a  $\text{SiO}_2/\text{Al}_2\text{O}_3$  molar ratio of 2.5 showed rather low 7- and 28-day compressive strengths (Fig. 7). When the molar ratio of  $\text{SiO}_2/\text{Al}_2\text{O}_3$  increased to 3.0, the compressive strengths were improved significantly. The 7-day compressive strength increased to 27.7 MPa for  $\text{Kln}_{750^\circ\text{C}}$ -based geopolymers, and increased to 58.7 MPa for  $\text{Hly}_{750^\circ\text{C}}$ -based geopolymers. This result demonstrated that increasing the  $\text{SiO}_2/\text{Al}_2\text{O}_3$  ratio could improve significantly the mechanical properties of geopolymers. When the  $\text{SiO}_2/\text{Al}_2\text{O}_3$  ratio increased to 3.5, the compressive strength of  $\text{Kln}_{750^\circ\text{C}}$ -based geopolymers increased slightly, whereas that of  $\text{Hly}_{750^\circ\text{C}}$ -based geopolymers decreased to 51.0 MPa, which may be attributed to the decreased alkalinity of the activator.  $\text{Hly}_{750^\circ\text{C}}$ -based geopolymers showed greater compressive strength than  $\text{Kln}_{750^\circ\text{C}}$ -based geopolymers,

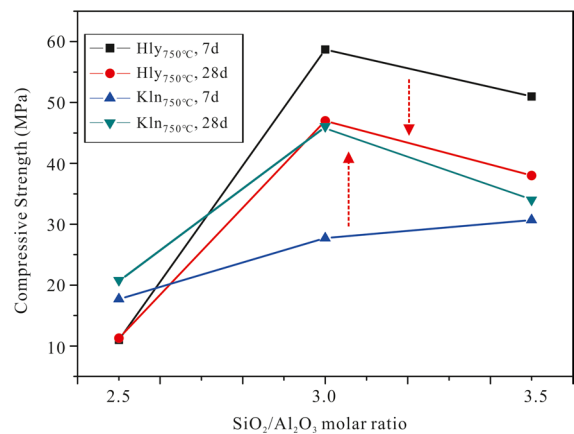


**Fig. 7** Compressive strength of  $\text{Kln}$ - and  $\text{Hly}$ -based geopolymers

resulting from the greater geopolymerization reactivity for Hly than Kln.

Note that, after 28 days of ageing, the compressive strength of Kln<sub>750°C</sub>-based geopolymer increased slightly; however, the compressive strength of Hly<sub>750°C</sub>-based geopolymers decreased, possibly because of the curing conditions. When cured at high temperature (80°C), Hly<sub>750°C</sub>-based geopolymeric paste hardened too fast to dissolve sufficiently, accompanied with fast evaporation of water, leading to the destruction of the geopolymer matrix. This process, therefore, may play a detrimental role in the development of compressive strength (Zhang et al., 2009, 2021). In comparison, Kln<sub>750°C</sub>-based geopolymers reacted continuously in the later stage of geopolymerization with improvement of compressive strength.

### Structure of Clay-based Geopolymers

#### XRD Results

The XRD patterns of Kln<sub>750°C</sub>-2.5 and Hly<sub>750°C</sub>-2.5 showed some reflections indexed to zeolite A with a  $d_{001}$  of 12.3 Å, which indicated that zeolite was formed (Fig. 8). In fact, previous reports found that geopolymers contained nanocrystalline zeolites, which can be crystallized under certain conditions, including high curing temperature, high humidity, etc. (Provis et al., 2005; Wang et al., 2017). Alkali-activation of Kln with a small Si/Al ratio induced the formation of zeolite easily. Qian et al. (2017) also found that zeolite A was formed after alkali-activation of metakaolinite at a Si/Al ratio of 1.0.

Hounsi and Lecomte (2013) studied alkali-activated Kln using 8 M NaOH solution and found that reyerite was formed. Similarly, Hly<sub>750°C</sub>-2.5 also contained zeolite A, but a smaller amount, according to the lower intensity of corresponding characteristic peaks (Fig. 8b). In addition, a broad reflection centered at  $27.7^\circ 2\theta$  was observed in the XRD patterns of Kln<sub>750°C</sub>-2.5 and Hly<sub>750°C</sub>-2.5. Compared to XRD patterns of Kln<sub>750°C</sub> and Hly<sub>750°C</sub> (Fig. 2), the center of the broad reflection shifted to higher regions after alkali-activation, which indicated that the network was reorganized and geopolymer had formed (Kaze et al., 2020a; Nkwaju et al., 2019).

When the SiO<sub>2</sub>/Al<sub>2</sub>O<sub>3</sub> ratio increased to >3.0, the zeolite crystal disappeared, accompanied by an increase in intensity of the broad peak centered at  $\sim 27.7^\circ 2\theta$ , indicating that the amount of amorphous geopolymer was increased. The quartz, however, remained intact after geopolymerization for Kln-based geopolymer due to its chemical stability.

These results demonstrated that the SiO<sub>2</sub>/Al<sub>2</sub>O<sub>3</sub> ratio affected the phase composition, which controlled the formation of zeolite or geopolymer for alkali-activated Kln<sub>750°C</sub> or Hly<sub>750°C</sub>. Their products showed no significant differences in the mineralogical phase under the same SiO<sub>2</sub>/Al<sub>2</sub>O<sub>3</sub> ratio, however.

#### FTIR Results

The absence of significant differences in local environments of the OH and other FTIR-active modes indicated that no significant differences

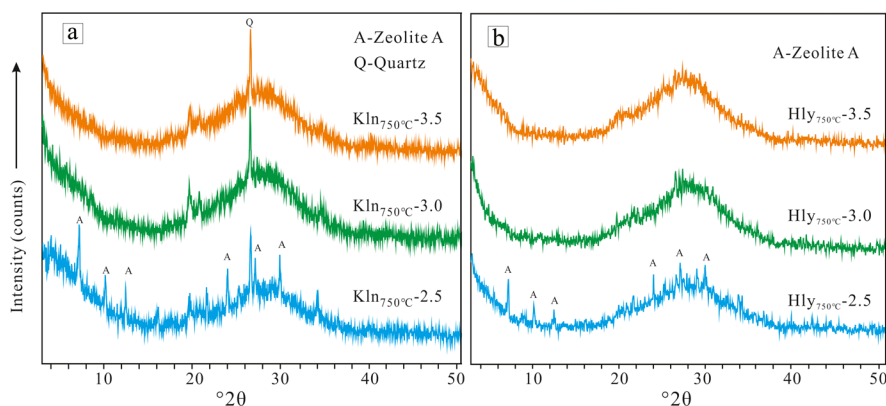


**Fig. 8** XRD patterns of **a** Kln- and **b** Hly-based geopolymers

transpired at the molecular scale between  $\text{Kln}_{750^\circ\text{C}}$  and  $\text{Hly}_{750^\circ\text{C}}$ -based geopolymers (Fig. 9). Furthermore, the peaks of the geopolymers were broad, which demonstrated that the alkali-activation products were highly amorphous.

The broad peaks in the range 3444 to 3464 and at  $1650\text{ cm}^{-1}$  were attributed to the stretching and bending vibrations of O–H from physically adsorbed water (Madejová & Komadel, 2001). The absorption at  $\sim 703\text{ cm}^{-1}$  corresponded to the bending vibration of Si–O–Al<sup>IV</sup>, while those at  $\sim 581$  and  $\sim 439\text{ cm}^{-1}$  should be associated with the stretching vibration of Al–O and the bending vibration of Si–O–Si, respectively. In addition, a shoulder observed at  $\sim 882\text{ cm}^{-1}$  was related to the presence of non-bridging-oxygens (e.g. Al–O–, Si–O–) resulting from the geopolymerization process.

Notably, for all geopolymers, a major band which appeared between  $1200$  and  $900\text{ cm}^{-1}$  was normally denoted the “main band,” which was attributed to an asymmetric stretching vibration of Si–O–T (T: Si or Al). This band has been used widely to investigate the chemical properties of geopolymers (Rees et al., 2007; Zhang et al., 2020a). Compared to FTIR spectra of  $\text{Kln}_{750^\circ\text{C}}$  and  $\text{Hly}_{750^\circ\text{C}}$  (Fig. 2), the main band shifted significantly to a lower wavenumber after

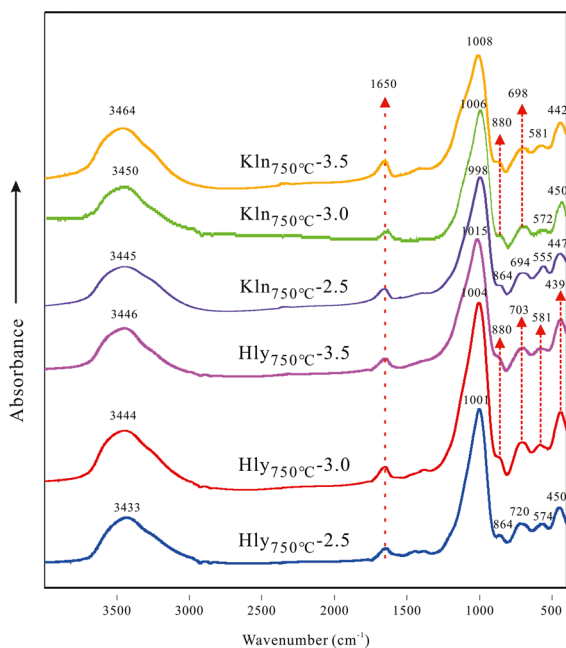


**Fig. 9** FTIR spectra of Kln- and Hly-based geopolymers

alkali-activation, owing to the increased amount of Si–OH and the substitution of Al in the silicate networks, leading to the decreased molecular vibrational force-constant (Rees et al., 2007; Zhang et al., 2020c). This displacement also reflected that Kln or Hly had dissolved and the geopolymers were formed. With the increase in the  $\text{SiO}_2/\text{Al}_2\text{O}_3$  ratio, the wavenumber of main bands for geopolymers increased slightly. This may be attributed to the incorporation of more Si into the geopolymer matrix or the more unreacted raw materials, which warrants further study (Bewa et al., 2020).

### NMR Results

The  $^{27}\text{Al}$  MAS NMR spectra of  $\text{Kln}_{750^\circ\text{C}}$  and  $\text{Hly}_{750^\circ\text{C}}$  (Fig. 10a) both showed three resonances centered at approximately 6, 31, and 59 ppm, which were assigned to Al<sup>VI</sup>, Al<sup>V</sup>, and Al<sup>IV</sup>, respectively. After reacting with alkaline solution, the  $^{27}\text{Al}$  MAS NMR spectra of all samples had a strong resonance at  $\sim 61$  ppm, accompanied by the disappearance of Al<sup>V</sup> and Al<sup>VI</sup>. Therefore, Al was mainly in four-coordination (Al<sup>IV</sup>) in the geopolymer despite the  $\text{SiO}_2/\text{Al}_2\text{O}_3$  ratios, indicating that increasing the  $\text{SiO}_2/\text{Al}_2\text{O}_3$  ratio did not significantly change the local structure of the Al environment in the geopolymer framework.

The  $^{29}\text{Si}$  CP/MAS NMR spectra of  $\text{Kln}_{750^\circ\text{C}}$  and  $\text{Hly}_{750^\circ\text{C}}$  showed one broad resonance centered at approximately  $-101$  ppm (Fig. 10b), which was attributed to a Q<sup>3</sup> Si environment, namely, Si was linked to three other Si atoms through oxygens (Maia et al., 2014). After geopolymerization, this peak shifted to a higher field position and decreased in intensity. This Si chemical shift was attributed to the Q<sup>4</sup>(mAl) environments, which was affected by Al substitution (Skibsted & Andersen, 2013). Previous studies have reported that for replacement of Si neighbors, as Q<sup>4</sup>(mAl), each additional  $[\text{AlO}_4]$  would increase the chemical shift by approximately 5 ppm (Walkley & Provis, 2019). Therefore, with the increase of  $\text{SiO}_2/\text{Al}_2\text{O}_3$  ratios, this peak shifted to lower field position.

Due to the fact that each peak centered between  $-86$  and  $90$  ppm was not unequivocally assignable to a single Si environment, Gaussian peak deconvolution of the  $^{29}\text{Si}$  NMR spectra for all geopolymers was conducted to analyze Q<sup>4</sup>(mAl) ( $0 \leq m \leq 4$ ) Si environments and obtain more specific information about

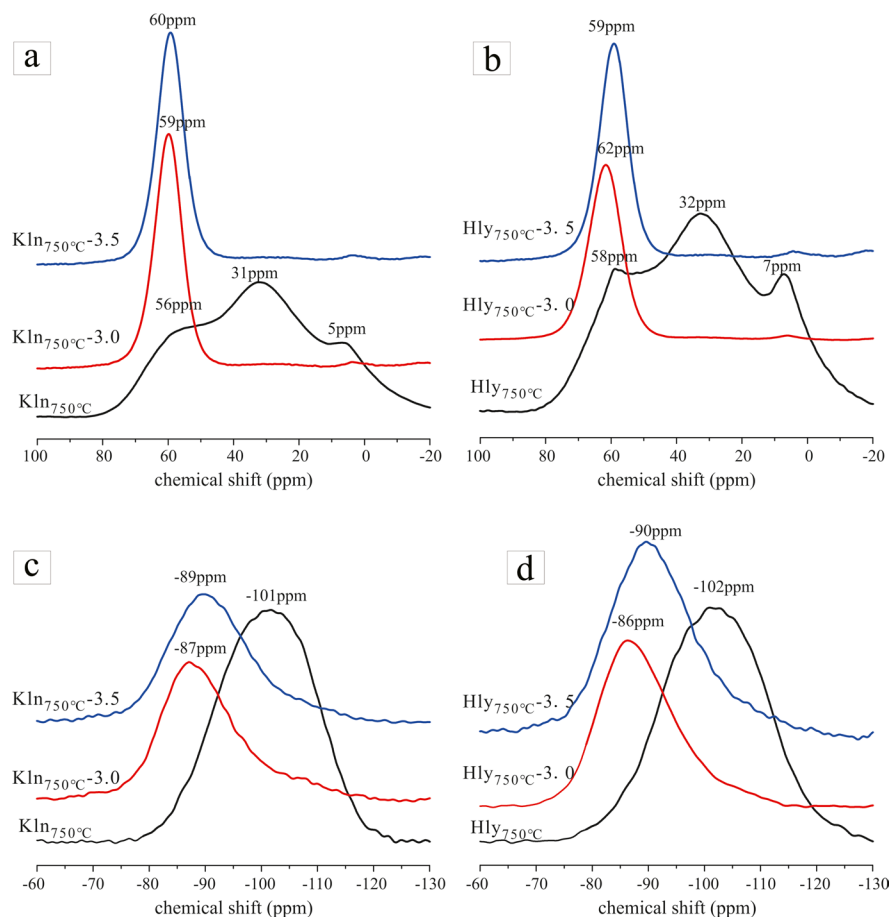


**Fig. 10**  $^{27}\text{Al}$  MAS NMR spectra of **a** Kln<sub>750°C</sub> and its alkali-activation products and **b** Hly<sub>750°C</sub> and its alkali-activation products;  $^{29}\text{Si}$  CP/MAS NMR spectra of **c** Kln<sub>750°C</sub> and its alkali-activation products; and **d** Hly<sub>750°C</sub> and its alkali-activation products

the Si coordination environments. Deconvolution of geopolymers produced five peaks located at approximately  $-108$ ,  $-100$ ,  $-93$ ,  $-87$ , and  $-80$  ppm (Fig. 11), which were attributed to  $\text{Q}^4(0\text{Al})$ ,  $\text{Q}^4(1\text{Al})$ ,  $\text{Q}^4(2\text{Al})$ ,  $\text{Q}^4(3\text{Al})$ , and  $\text{Q}^4(4\text{Al})$ , respectively.

All geopolymers consisted mainly of  $\text{Q}^4(2\text{Al})$  and  $\text{Q}^4(3\text{Al})$  (Table 3), which demonstrated that one  $[\text{SiO}_4]$  tetrahedron connected mainly to two or three  $[\text{AlO}_4]$  tetrahedra in this geopolymer network. In addition, the fraction of  $\text{Q}^4(\text{mAl})$  structural units rich in Si (i.e.  $\text{Q}^4(0\text{Al})$ ,  $\text{Q}^4(1\text{Al})$ , and  $\text{Q}^4(2\text{Al})$ ) increased as the  $\text{SiO}_2/\text{Al}_2\text{O}_3$  ratios increased. When the  $\text{SiO}_2/\text{Al}_2\text{O}_3$  ratios increased from 3.0 to 3.5, the value of  $(\text{Q}^4(0\text{Al}) + \text{Q}^4(1\text{Al}) + \text{Q}^4(2\text{Al})) / (\text{Q}^4(4\text{Al}) + \text{Q}^4(3\text{Al}))$  increased from 0.77 to 1.29 and from 1.17 to 2.43 for Kln-based and Hly-based geopolymers, respectively. At the same  $\text{SiO}_2/\text{Al}_2\text{O}_3$  ratio, the geopolymers derived

from Hly contained more Si than those derived from Kln, which may be one reason why Hly-based geopolymers exhibited better properties than Kln-based geopolymers (He et al., 2016; Qian et al., 2017).

### SEM Results

Scanning electron micrographs (Fig. 12a) revealed that Hly<sub>750°C</sub>-2.5 exhibited a rather loosely bonded microstructure with some macropores and cracks, which corresponded to the low compressive strength. At high magnification, some nanotubular species were loosely stacked together without the formation of continuous integrity (Fig. 12d). These nanotubular species should be the unreacted Hly<sub>750°C</sub> resulting from incomplete dissolution. In addition, some prismatic particles formed, which were comprised mainly

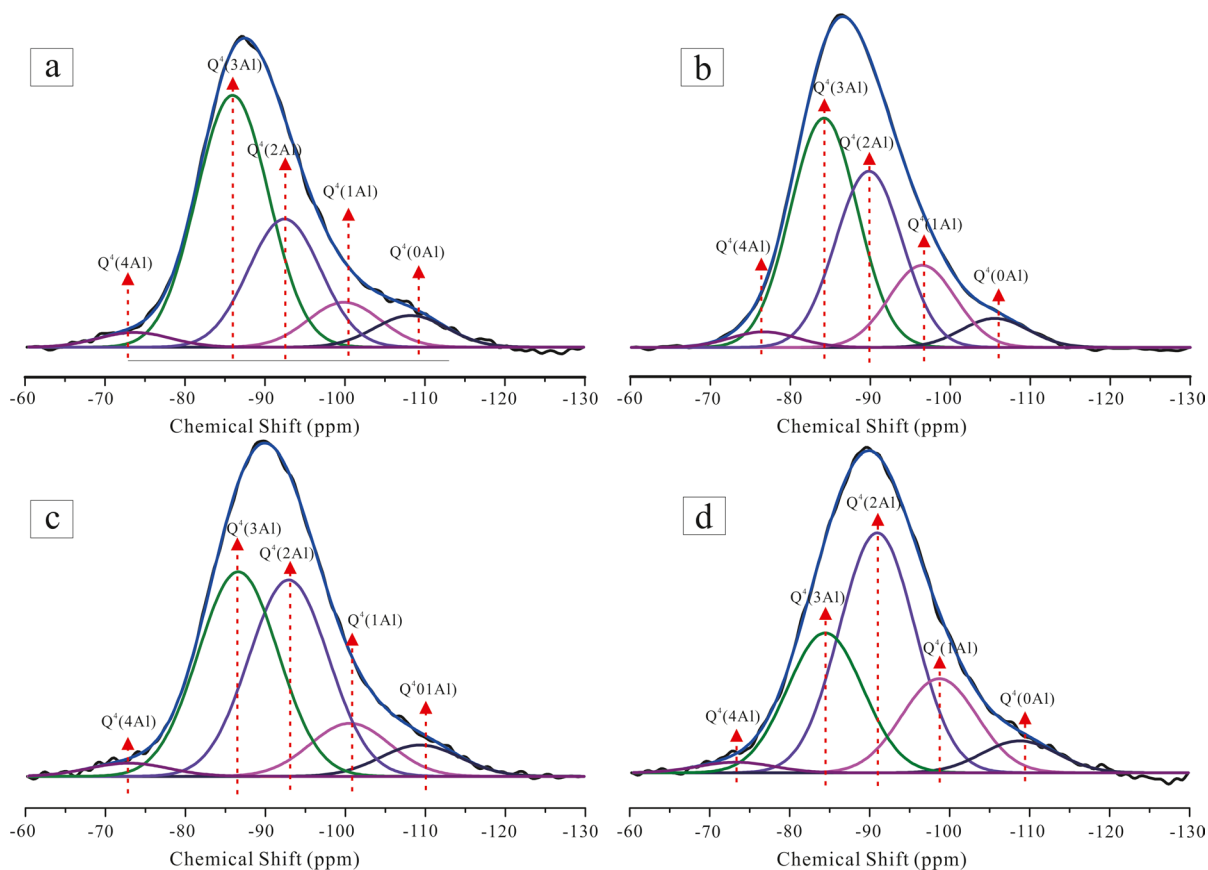


**Fig. 11** Deconvolution results for  $^{29}\text{Si}$  CP/MAS NMR spectra of clay-based geopolymers: **a**  $\text{Kln}_{750^\circ\text{C}}\text{-3.0}$ ; **b**  $\text{Kln}_{750^\circ\text{C}}\text{-3.5}$ ; **c**  $\text{Hly}_{750^\circ\text{C}}\text{-3.0}$ ; and **d**  $\text{Hly}_{750^\circ\text{C}}\text{-3.5}$

**Table 3** Fractional areas of the constituent NMR peaks

| Samples                                     | $^{29}\text{Si}$  | $\text{Q}^4(0\text{Al})$ | $\text{Q}^4(1\text{Al})$ | $\text{Q}^4(2\text{Al})$ | $\text{Q}^4(3\text{Al})$ | $\text{Q}^4(4\text{Al})$ |
|---|-------------------|--------------------------|--------------------------|--------------------------|--------------------------|--------------------------|
| $\text{Kln}_{750^\circ\text{C}}\text{-3.0}$ | $\delta$ (ppm)    | -108.2                   | -99.9                    | -92.4                    | -86.0                    | -73.3                    |
|   | Relative area (%) | 6.72                     | 9.53                     | 27.2                     | 53.4                     | 3.12                     |
|   | FWHM              | 10.63                    | 10.63                    | 10.63                    | 10.63                    | 10.63                    |
| $\text{Kln}_{750^\circ\text{C}}\text{-3.5}$ | $\delta$ (ppm)    | -109.3                   | -100.7                   | -92.9                    | -86.6                    | -72.9                    |
|   | Relative area (%) | 6.27                     | 10.63                    | 39.41                    | 41.04                    | 2.64                     |
|   | FWHM              | 11.74                    | 11.74                    | 11.74                    | 11.74                    | 11.74                    |
| $\text{Hly}_{750^\circ\text{C}}\text{-3.0}$ | $\delta$ (ppm)    | -106.9                   | -97.8                    | -90.5                    | -85.3                    | -78.1                    |
|   | Relative area (%) | 5.45                     | 15.43                    | 33.12                    | 43.08                    | 2.92                     |
|   | FWHM              | 9.81                     | 9.81                     | 9.81                     | 9.81                     | 9.81                     |
| $\text{Hly}_{750^\circ\text{C}}\text{-3.5}$ | $\delta$ (ppm)    | -108.7                   | -98.7                    | -90.9                    | -84.4                    | -73.3                    |
|   | Relative area (%) | 6.18                     | 18.23                    | 46.46                    | 27.09                    | 2.04                     |
|   | FWHM              | 11.08                    | 11.08                    | 11.08                    | 11.08                    | 11.08                    |

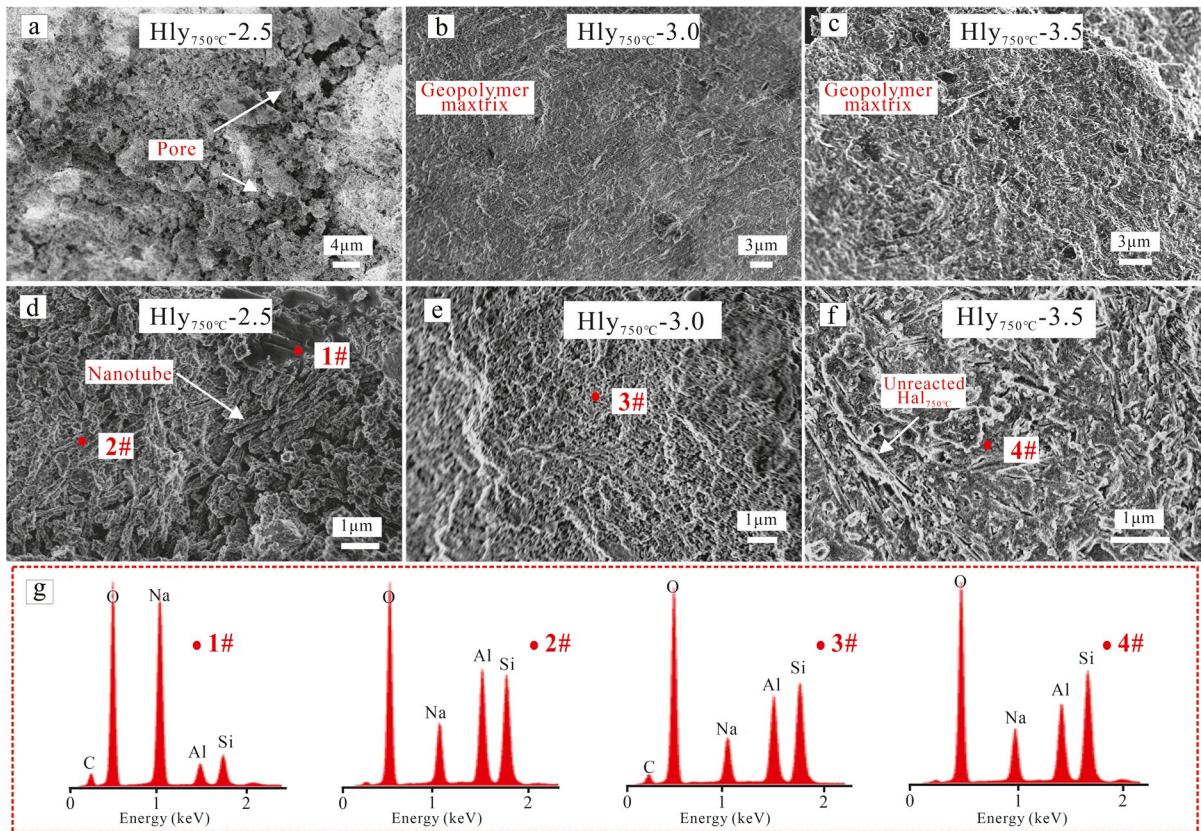


**Fig. 12** SEM images of Hly- and Kln-based geopolymers: **a, d** Hly<sub>750°C</sub>-2.5; **b, e** Hly<sub>750°C</sub>-2.0; **c, f** Hly<sub>750°C</sub>-3.5; **g** EDX result of Hly-based geopolymer; **h, l** Kln<sub>750°C</sub>-2.5; **i, m** Kln<sub>750°C</sub>-3.0; **k, n** Kln<sub>750°C</sub>-3.5

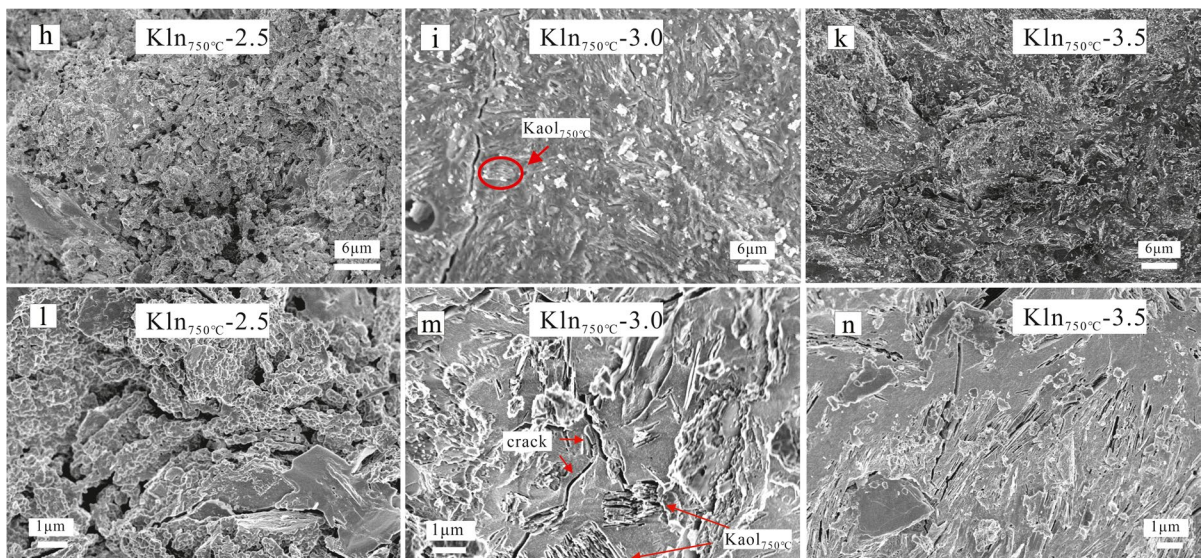


**Fig. 12** (continued)

of Na and O with traces of C, Si, and Al elements according to EDX analysis (Fig. 12g, #1). This particle should be attributed mainly to the NaOH, while a small amount of  $\text{Na}_2\text{CO}_3$  formed through the reaction between NaOH and atmospheric  $\text{CO}_2$ . Similarly,  $\text{Kln}_{750^\circ\text{C}}\text{-2.5}$  also had a rather uncompact and inhomogeneous microstructure (Fig. 12h,k), which thus exhibited low compressive strength.

$\text{Hly}_{750^\circ\text{C}}\text{-3.0}$  had significant continuity texture with an homogeneous and compact microstructure (Fig. 12b,e). The densification of alkali-activated products was consistent with the improvements in compressive strength of the geopolymers. The EDX analysis showed that the geopolymer matrix was composed mainly of Na, Si, Al, and O elements, indicating the formation of sodium aluminosilicate hydrate (N–A–S–H). In Fig. 12c,  $\text{Hly}_{750^\circ\text{C}}\text{-3.5}$  still showed a compact microstructure with micropores. However, unreacted  $\text{Hly}_{750^\circ\text{C}}$  was still embedded in the geopolymer matrix (Fig. 12f), causing the less homogeneous structure of  $\text{Hly}_{750^\circ\text{C}}\text{-3.5}$  and decreased the compressive strength.

Notably, the microstructure of geopolymers derived from  $\text{Kln}_{750^\circ\text{C}}$  was obviously less homogeneous and less compact than from  $\text{Hly}_{750^\circ\text{C}}$  under the same conditions. Many unreacted  $\text{Kln}_{750^\circ\text{C}}$  crystallites were easily found to be embedded in the geopolymeric matrix, which caused the formation of many cracks and destroyed significantly the homogenous structure of the geopolymer (Fig. 12l,m). This may account for the lower 7-day

compressive strength of  $\text{Kln}_{750^\circ\text{C}}$  compared to  $\text{Hly}_{750^\circ\text{C}}$ -based geopolymers. However, further studies and more technologies are required to research the similar 28-day strengths between  $\text{Kln}_{750^\circ\text{C}}$ - and  $\text{Hly}_{750^\circ\text{C}}$ -based geopolymers.

These results also confirmed that the soluble  $\text{SiO}_2$  was very important for the geopolymer formation. The lack of soluble  $\text{SiO}_2$  would inhibit the dissolution of minerals and impede the polycondensation of  $[\text{SiO}_4]$  and  $[\text{AlO}_4]$  oligomers even using a very highly alkaline solution for alkali-activation (Liew et al., 2016; Singh et al., 2005). On the other hand, the morphological differences between  $\text{Kln}$  and  $\text{Hly}$  also affect the microstructure of the geopolymers. Nanotubular  $\text{Hly}$  appeared to possess greater geopolymerization reactivity than platy  $\text{Kln}$  according to the more compact and homogeneous microstructure for  $\text{Hly}_{750^\circ\text{C}}$  than for  $\text{Kln}_{750^\circ\text{C}}$ -based geopolymers.

#### Pore Distribution

The pore-size distribution curves of all geopolymers in Fig. 13a exhibited a unimodal distribution. A broad peak occurred in the range from 10–100 nm with a center at 35 nm, which was attributed to capillary pores in the geopolymer matrix (Ma et al., 2013). The broader-shaped peak of  $\text{Kln}_{750^\circ\text{C}}$ -based geopolymer rather than the narrower  $\text{Hly}_{750^\circ\text{C}}$ -based peak indicated that the pore distribution of  $\text{Kln}_{750^\circ\text{C}}$ -based geopolymer has a lower degree of homogeneity than that of  $\text{Hly}_{750^\circ\text{C}}$ -based geopolymer. Furthermore, the  $\text{SiO}_2/\text{Al}_2\text{O}_3$  ratio was poorly

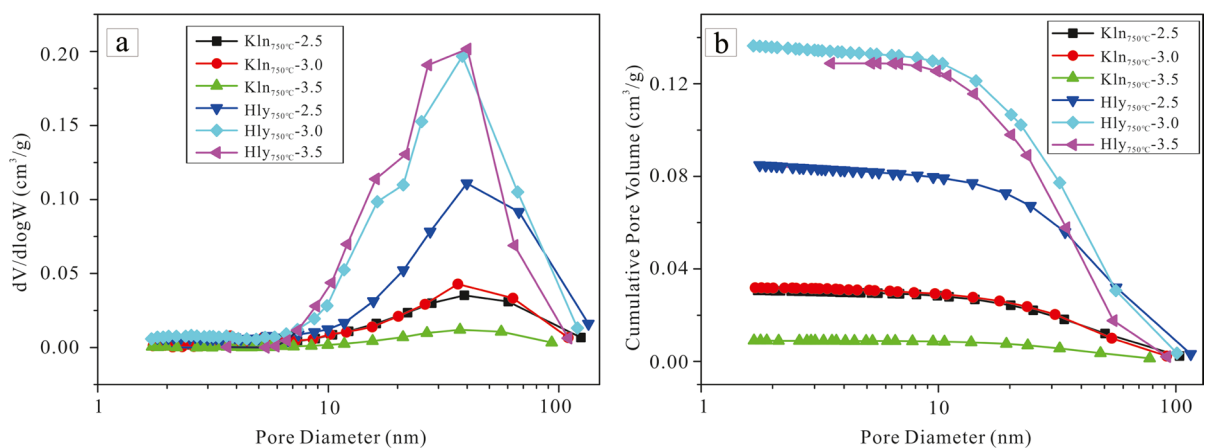


**Fig. 13** a Pore-size distribution and b cumulative pore volume of clay-based geopolymers

related to the pore-size distribution and cumulative pore volume, at least in the mesopore range. This was shown by the similar average pore diameters of all the geopolymers (~23 nm) (Table 4).

It is of note that although the pore volume of the Kln<sub>750°C</sub>-based geopolymer was less than that of the Hly<sub>750°C</sub>-based geopolymer (Table 4), Kln<sub>750°C</sub>-based geopolymer exhibited lower compressive strength than Hly<sub>750°C</sub>-based geopolymer. Table 4 also shows that Kln<sub>750°C</sub>-based geopolymers had much lower specific surface area than Hly<sub>750°C</sub>-based geopolymers, which demonstrated that Hly<sub>750°C</sub>-based geopolymers may possess more pores (micropore and mesopore) than Kln<sub>750°C</sub>-based ones. This result revealed that, at least in the mesopore range, porosity has no direct relation with compressive strength. As observed from SEM images, many macropores and cracks were present in the Kln<sub>750°C</sub>-based geopolymer matrix (Fig. 12e,f), but these macropores or cracks could not be characterized by N<sub>2</sub> physisorption analysis, which was also an important factor influencing the compressive strength. On the other hand, the presence of the unreacted particles (e.g. NaOH, Na<sub>2</sub>SiO<sub>4</sub>) would cover the surface of a geopolymer, thus reducing the pore volume (Zhang et al., 2020c).

## General Discussion

Recently, owing to its special microstructure and high reactivity, the use of Hly for preparation of geopolymers has attracted increasing attention (Kaze et al., 2018; Blaise et al., 2019; Zhang et al., 2021; Martina

et al., 2022; Navid et al., 2023). Kaze et al. (2018) investigated the effects of NaOH concentration on the properties of Hly<sub>600°C</sub>-based geopolymers. As the NaOH concentration increased, the compressive strengths increased at first and then decreased. When NaOH concentration increased to 10 mol/L, the compressive strength reached 28 MPa. However, the detailed SiO<sub>2</sub>/Al<sub>2</sub>O<sub>3</sub> ratio of raw materials was unclear. The same authors also compared mechanical and thermal properties of Hly and Kln (Kaze et al., 2022; Tchakouté et al., 2020) and concluded that Hly-based geopolymer showed better properties than Kln-based geopolymer because Hly possessed a smaller particle size and greater specific surface area than Kln. However, the calcined Hly they used was spherical; this may result in different geopolymerization behavior in contrast to Hly with a nanotubular shape. For example, they stated that the spherical shapes of Hly could provide nucleation sites necessary to bolster the geopolymerization process, which sites were not found in the current study. Besides, the clays (three kinds) used in Kaze's study contained many impurities, such as illite, anatase, and quartz and the calcination of clays was incomplete, which may influence the geopolymerization of Hly. In addition, Zhang et al. (2021) compared various curing conditions on the mechanical properties and microstructure of Hly-based geopolymers and found that as the curing temperature increased to ≥50°C, the compressive strengths decreased with ageing time. This is consistent with the present study, in which the compressive strength of Hly-based geopolymers decreased with ageing. In contrast, the compressive strength of Kln-based geopolymers increased with ageing, which confirmed that the optimal curing condition is related to the reactivity of precursors and high curing temperature is not suitable for highly reactive precursors.

Many other studies have been carried out concerning the improved properties of Hly-based geopolymers (Blaise et al., 2019; Zhang et al., 2020b; Kaze et al., 2021), utilization of Hly as an additive in geopolymers (Kaze et al., 2020b; Nemaleu et al., 2021; Navid et al., 2023), and application of Hly-based geopolymers (Barrie et al., 2015; Martina et al., 2022). However, these studies focused more on the properties of Hly-based or Hly-related geopolymers than on the nanotubular morphology of Hly in geopolymerization, which is interesting clay-related research. Although nanotubular Hly shows similar

**Table 4** Pore parameters and specific surface area of geopolymers

| Samples                   | Average pore diameter (nm) | Total pore area (m <sup>2</sup> /g) | Specific surface area (m <sup>2</sup> /g) |
|---------------------------|----------------------------|-------------------------------------|---|
| Kln <sub>750°C</sub> -2.5 | 21.39                      | 0.031                               | 5.97                                      |
| Kln <sub>750°C</sub> -3.0 | 21.78                      | 0.032                               | 4.01                                      |
| Kln <sub>750°C</sub> -3.5 | 25.31                      | 0.0090                              | 1.42                                      |
| Hly <sub>750°C</sub> -2.5 | 23.73                      | 0.085                               | 14.65                                     |
| Hly <sub>750°C</sub> -3.0 | 22.07                      | 0.14                                | 20.95                                     |
| Hly <sub>750°C</sub> -3.5 | 24.84                      | 0.13                                | 16.10                                     |

chemical composition to plate-like Kln, their microstructures and morphologies are quite different. These differences between Kln and Hly also cause the different physicochemical properties. Therefore, Hly shows not only similar but also different behavior to Kln during alkali-activation.

The results obtained demonstrated that, as with Kln, the alkali-activation products from Hly were zeolite A and the geopolymer when the  $\text{SiO}_2/\text{Al}_2\text{O}_3$  ratio was 2.5. Owing to the formation of different phases with large amounts of pores, the alkali-activation products derived from Kln and Hly both showed low compressive strength. Likewise, when  $\text{SiO}_2/\text{Al}_2\text{O}_3$  ratio was increased to  $>3.0$ , the alkali-activation of Hly produced mainly geopolymers analogous to the alkali-activated Kln-based geopolymers. Sufficient amounts of soluble  $\text{SiO}_2$  induced the polycondensation of oligomers to form geopolymers with compact and homogeneous structures (Ferone et al., 2015; Valentini, 2018), which improved the compressive strength.

However, the above findings also indicated that the microstructure of the Hly-based geopolymer differed significantly from the Kln-based geopolymer. This phenomenon can be attributed to the different

morphologies of Kln and Hly. As mentioned above, Kln consisted of stacked repeating layers to form a platy morphology. Normally, the particle size of Kln is a few microns, and the lamellar thickness is hundreds or thousands of nanometers. In contrast, Hly usually adopts a rolling of the unit layer to form a tubular morphology. The diameter of the tubular particles is nanometers, while the thickness of the tubular wall is a few nanometers, which is much smaller than that of Kln (Yuan et al., 2015). According to Davidovits (2011), the Kln is attacked by alkaline solution at the edge and basal surfaces and inside the structure, layer by layer, during geopolymerization. Many unreacted Kln particles were present in Kln-based geopolymers due to insufficient dissolution. However, for Hly, both outside and inside surfaces of the Hly nanotube can be attacked by alkaline solution (Fig. 14), the dissolution of Si and Al from Hly was, thus, easier and quicker than from Kln, which was confirmed by the dissolution results (Table 2). This may accelerate the alkali-activation to improve the geopolymerization degree at an early stage (Fig. 6).

Significantly, the different structures between Kln and Hly might also cause the different

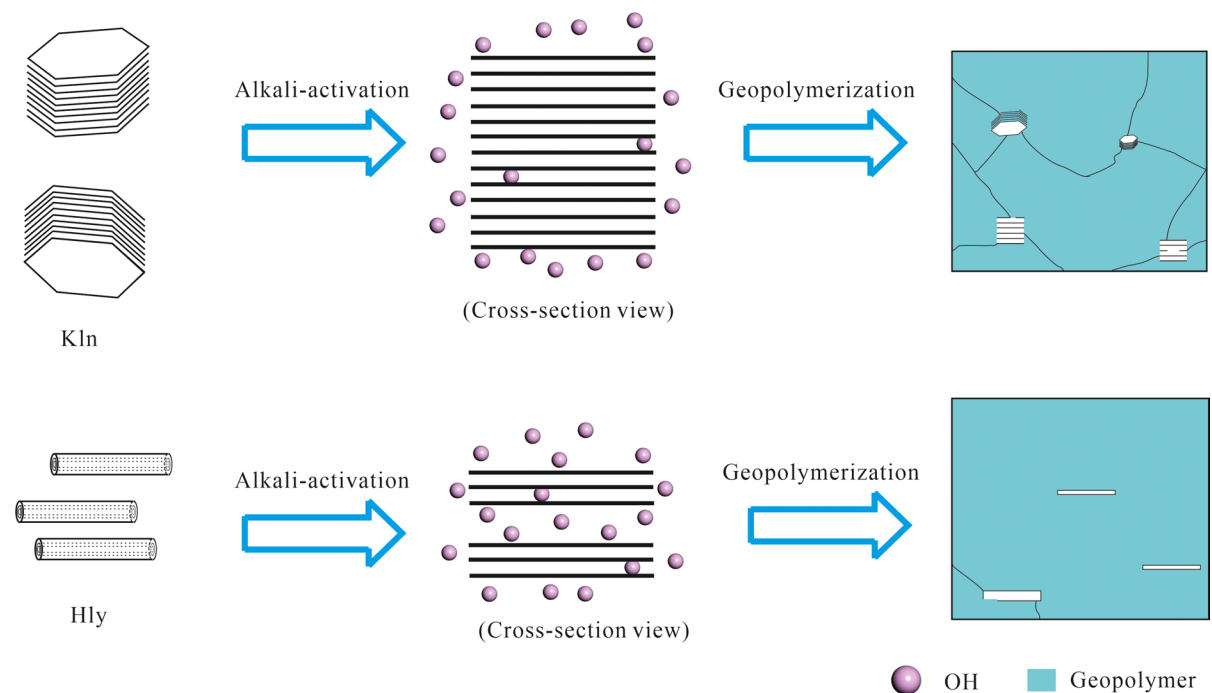


**Fig. 14** Schematic diagram of alkali-activated Kln- and Hly-based geopolymers

geopolymerization reactivity. Compared to Kln, the formation of naturally occurring Hly is prone to form defects under geological effects (Joussein et al., 2005). Therefore, the degree of structural ordering of nanotubular Hly is obviously lower than that of plate-like Kln, resulting in the greater reactivity for Hly than Kln. On the other hand, Hly has a larger specific surface area than Kln, which can provide more contact sites for activators, leading to more release of Si and Al and, thus, a greater degree of geopolymerization than Kln (Zhang et al., 2012a).

Furthermore, the unique properties of Hly might also cause different geopolymerization behavior from Kln. For example, previous reports indicated that the unit mass of the number of surface active points in Hly is greater than that of Kln (Tan et al., 2015; Yuan et al., 2008). In addition, the outer surfaces of the nanotubes of Hly will form hydroxyl groups after calcination at 600–900°C; however, no similar reports have been made about the calcination of Kln (Yuan et al., 2012). These effects on the microstructure and composition of as-synthesized geopolymers should also be considered in future studies.

## Conclusions

The dependence of the microstructure and compressive strength of geopolymers derived from platy kaolinite and nanotubular halloysite on the  $\text{SiO}_2/\text{Al}_2\text{O}_3$  ratio was investigated here by means of a combination of spectroscopic and microscopic techniques. When the  $\text{SiO}_2/\text{Al}_2\text{O}_3$  ratio was 2.5, both alkali-activated kaolinite and alkali-activated halloysite exhibited a loosely bound and inhomogeneous microstructure due to the formation of zeolite A. When the  $\text{SiO}_2/\text{Al}_2\text{O}_3$  ratio was 3 or 3.5, the alkali-activation product was a geopolymer which showed compact and dense microstructure with high compressive strength.

In addition, compared to kaolinite-based geopolymers, the microstructure of halloysite-based geopolymers was more compact and homogeneous, and with fewer unreacted particles, which thus exhibited greater early compressive strength. This can be attributed to the different morphologies between halloysite and kaolinite. Halloysite possesses a nanosized tubular morphology, which showed a smaller particle size and larger specific surface area than kaolinite. Therefore, the  $\text{OH}^-$  can attack readily the halloysite

tube from both the inside and outside surfaces, leaching more Si and Al, and forming larger amounts of geopolymer. Moreover, the nanosized particles did not destroy significantly the geopolymer matrix, which results in a better mechanical performance for halloysite-based geopolymers than kaolinite-based geopolymers.

These findings indicated that the mechanical properties and microstructure of clay-based geopolymers are not only influenced by the  $\text{SiO}_2/\text{Al}_2\text{O}_3$  ratio but also by the microstructure and morphology of the raw materials. Nanotubular halloysite is a promising geopolymer precursor, which showed greater geopolymerization reactivity than plate-like kaolinite.

**Acknowledgements** Financial support by the National Special Support for High-Level Personnel, Basic and Applied Basic Research Foundation of Guangdong Province (Grant No 2023A1515012180), and the National Natural Science Foundation of China (Grant Nos. 52161145405 and 41972045) are gratefully acknowledged.

**Data Availability** Data will be available on request.

## Declarations

**Competing Interest** The authors declare that there is no conflict of interest.

## References

- Amran, Y. H. M., Alyousef, R., Alabduljabbar, H., & El-Zeadani, M. (2020). Clean production and properties of geopolymer concrete; A review. *Journal of Cleaner Production*, 251, 119679. <https://doi.org/10.1016/j.jclepro.2019.119679>
- Barrie, E., Cappuyns, V., Vassilieva, E., Adriaens, R., Hollanders, S., Garcés, D., Paredes, C., Pontikes, Y., Elsen, J., & Machiels, L. (2015). Potential of inorganic polymers (geopolymers) made of halloysite and volcanic glass for the immobilisation of tailings from gold extraction in Ecuador. *Applied Clay Science*, 109–110, 95–106. <https://doi.org/10.1016/j.clay.2015.02.025>
- Bewa, C. N., Tchakouté, H. K., Banenzoué, C., Cakanou, L., Mbakop, T. T., Kamseu, E., & Rüscher, C. H. (2020). Acid-based geopolymers using waste fired brick and different metakaolins as raw materials. *Applied Clay Science*, 198, 105813. <https://doi.org/10.1016/j.clay.2020.105813>
- Blaise, N. B., Ndigui, B., Emmanuel, Y., Rodrigue, C. K., & Robert, N. (2019). Effect of limestone dosages on some properties of geopolymer from thermally activated halloysite. *Construction and Building Materials*, 217, 28–35. <https://doi.org/10.1016/j.conbuildmat.2019.05.058>
- Cai, J., Tan, J., & Li, X. (2020). Thermoelectric behaviors of fly ash and metakaolin based geopolymer. *Construction*

- and *Building Materials*, 237, 117757. <https://doi.org/10.1016/j.conbuildmat.2019.117757>
- Chen, K., Wu, D., Xia, L., Cai, Q., & Zhang, Z. (2021). Geopolymer concrete durability subjected to aggressive environments – A review of influence factors and comparison with ordinary Portland cement. *Construction and Building Materials*, 279, 122496. <https://doi.org/10.1016/j.conbuildmat.2021.122496>
- Davidovits, J. (2011). *Geopolymer Chemistry and Applications*. 3rd Edition, Institut Geopolymere, Saint-Quentin.
- Deng, L., Yuan, P., Liu, D., Annabi-Bergaya, F., Zhou, J., Chen, F., & Liu, Z. (2017). Effects of microstructure of clay minerals, montmorillonite, kaolinite and halloysite, on their benzene adsorption behaviors. *Applied Clay Science*, 143, 184–191. <https://doi.org/10.1016/j.clay.2017.03.035>
- Duxson, P., Mallicoat, S. W., Lukey, G. C., Kriven, W. M., & Deventer, J. S. J. (2007). The effect of alkali and Si/Al ratio on the development of mechanical properties of metakaolin-based geopolymers. *Colloids and Surfaces A: Physicochemical and Engineering Aspects*, 292, 8–20. <https://doi.org/10.1016/j.colsurfa.2006.05.044>
- Farhan, N. A., Sheikh, M. N., & Hadi, M. N. S. (2019). Investigation of engineering properties of normal and high strength fly ash based geopolymer and alkali-activated slag concrete compared to ordinary Portland cement concrete. *Construction and Building Materials*, 196, 26–42. <https://doi.org/10.1016/j.conbuildmat.2018.11.083>
- Ferone, C., Liguori, B., Capasso, I., Colangelo, F., Cioffi, R., Cappelletto, E., & Di Maggio, R. (2015). Thermally treated clay sediments as geopolymer source material. *Applied Clay Science*, 107, 195–204. <https://doi.org/10.1016/j.clay.2015.01.027>
- Haw, T. T., Hart, F., Rashidi, A., & Pasbakhsh, P. (2020). Sustainable cementitious composites reinforced with metakaolin and halloysite nanotubes for construction and building applications. *Applied Clay Science*, 188, 105533. <https://doi.org/10.1016/j.clay.2020.105533>
- He, J., Zhang, J., Yu, Y., & Zhang, G. (2012). The strength and microstructure of two geopolymers derived from metakaolin and red mud-fly ash admixture: A comparative study. *Construction and Building Materials*, 30, 80–91. <https://doi.org/10.1016/j.conbuildmat.2011.12.011>
- He, P., Wang, M., Shuai, F., Jia, D., Shu, Y., Yuan, J., Xu, J., Wang, P., & Yu, Z. (2016). Effects of Si/Al ratio on the structure and properties of metakaolin based geopolymer. *Ceramics International*, 42, 14416–14422. <https://doi.org/10.1016/j.ceramint.2016.06.033>
- Heah, C. Y., Kamarudin, H., Al Bakri, A. M. M., Bnhussain, M., Luqman, M., Nizar, I. K., Ruzaidi, C. M., & Liew, Y. M. (2012). Study on solids-to-liquid and alkaline activator ratios on kaolin-based geopolymers. *Construction and Building Materials*, 35, 912–922. <https://doi.org/10.1016/j.conbuildmat.2012.04.102>
- Hollanders, S., Adriaens, R., Skibsted, J., Cizer, Ö., & Elsen, J. (2016). Pozzolanic reactivity of pure calcined clays. *Applied Clay Science*, 132–133, 552–560. <https://doi.org/10.1016/j.clay.2016.08.003>
- Hounsi, A. D., & Lecomte, G. L. (2013). Kaolin-based geopolymers: Effect of mechanical activation and curing process. *Construction and Building Materials*, 42, 105–113. <https://doi.org/10.1016/j.conbuildmat.2012.12.069>
- Hu, N., Bernsmeier, D., Grathoff, G. H., & Warr, L. N. (2016). The influence of alkali activator type, curing temperature and gibbsite on the geopolymerization of an interstratified illite-smectite rich clay from Friedland. *Applied Clay Science*, 135, 386–393. <https://doi.org/10.1016/j.clay.2016.10.021>
- Izadifar, M., Thissen, P., Steudel, A., Kleeberg, R., Kaufhold, S., Kaltenbach, J., Schuhmann, R., Dehn, F., & Emmerich, K. (2020). Comprehensive examination of dehydroxylation of kaolinite, disordered kaolinite, and dickite: Experimental studies and density functional theory. *Clays and Clay Minerals*, 68, 319–333. <https://doi.org/10.1007/s42860-020-00082-w>
- Joussein, E., Petit, S. G., Churchman, J., Theng, B. K. G., Righi, D., & Delvaux, B. (2005). Halloysite clay minerals – A review. *Clay Minerals*, 40, 383–426. <https://doi.org/10.1180/0009855054040180>
- Kaze, C. R., Tchakoute, H. K., Mbakop, T. T., Mache, J. R., Kamseu, E., Melo, U. C., Leonelli, C., & Rahier, H. (2018). Synthesis and properties of inorganic polymers (geopolymers) derived from Cameroon-meta-halloysite. *Ceramics International*, 44, 18499–18508. <https://doi.org/10.1016/j.ceramint.2018.07.070>
- Kaze, C. R., Alomayri, T., Hasan, A., Tome, S., Lecomte-Nana, G. L., Nemaleu, J. G. D., Tchakoute, H. K., Kamseu, E., Melo, U. C., & Rahier, H. (2020). Reaction kinetics and rheological behaviour of meta-halloysite based geopolymer cured at room temperature: Effect of thermal activation on physicochemical and microstructural properties. *Applied Clay Science*, 196, 105773. <https://doi.org/10.1016/j.clay.2020.105773>
- Kaze, C. R., Venyite, P., Nana, A., Deutou, J. G. N., Tchakoute, H. K., Rahier, H., Kamseu, E., Melo, U. C., & Leonelli, C. (2020). Meta-halloysite to improve compactness in iron-rich laterite-based alkali activated materials. *Materials Chemistry and Physics*, 239, 122268. <https://doi.org/10.1016/j.matchemphys.2019.122268>
- Kaze, C. R., Adesina, A., Alomayri, T., Assaedi, H., Kamseu, E., Melo, U. C., Andreola, F., & Leonelli, C. (2021). Characterization, reactivity and rheological behaviour of metakaolin and Meta-halloysite based geopolymer binders. *Cleaner Materials*, 2, 100025. <https://doi.org/10.1016/j.clema.2021.100025>
- Kaze, C. R., Nana, A., Lecomte-Nana, G. L., Deutou, J. G. N., Kamseu, E., Melo, U. C., Andreola, F., & Leonelli, C. (2022). Thermal behaviour and microstructural evolution of metakaolin and meta-halloysite-based geopolymer binders: A comparative study. *Journal of Thermal Analysis and Calorimetry*, 147(3), 2055–2071. <https://doi.org/10.1007/s10973-021-10555-2>
- Khalifa, A. Z., Cizer, Ö., Pontikes, Y., Heath, A., Patureau, P., Bernal, S. A., & Marsh, A. T. M. (2020). Advances in alkali-activation of clay minerals. *Cement and Concrete Research*, 132, 106050. <https://doi.org/10.1016/j.cemconres.2020.106050>
- Li, Y., Chen, M., Song, H., Yuan, P., Liu, D., Zhang, B., & Bu, H. (2020). Methane hydrate formation in the stacking of kaolinite particles with different surface contacts as nano-reactors: A molecular dynamics simulation study. *Applied Clay Science*, 186, 105439. <https://doi.org/10.1016/j.clay.2020.105439>

- Liew, Y. M., Heah, C. Y., Al Bakri, M. M., & Hussin, K. (2016). Structure and properties of clay-based geopolymer cements: A review. *Progress in Materials Science*, *83*, 595–629. <https://doi.org/10.1016/j.pmatsci.2016.08.002>
- Liu, J., Zha, F., Xu, L., Kang, B., Yang, C., Zhang, W., Zhang, J., & Liu, Z. (2020). Zinc leachability in contaminated soil stabilized/solidified by cement-soda residue under freeze-thaw cycles. *Applied Clay Science*, *186*, 105474. <https://doi.org/10.1016/j.clay.2020.105474>
- Liu, J., Doh, J., Dinh, H. L., Ong, D. E. L., Zi, G., & You, I. (2022). Effect of Si/Al molar ratio on the strength behavior of geopolymer derived from various industrial waste: A current state of the art review. *Construction and Building Materials*, *329*, 127134. <https://doi.org/10.1016/j.conbuildmat.2022.127134>
- Lolli, F., Manzano, H., Provis, J. L., Bignozzi, M. C., & Masoero, E. (2018). Atomistic Simulations of Geopolymer Models: The Impact of Disorder on Structure and Mechanics. *ACS Applied Materials & Interfaces*, *10*, 22809–22820. <https://doi.org/10.1021/acsami.8b03873>
- Ma, Y., Hu, J., & Ye, G. (2013). The pore structure and permeability of alkali activated fly ash. *Fuel*, *104*, 771–780. <https://doi.org/10.1016/j.fuel.2012.05.034>
- Madejová, J., & Komadel, P. (2001). Baseline studies of the clay minerals society source clays: Infrared methods. *Clays and Clay Minerals*, *49*, 372–373. <https://doi.org/10.1346/CCMN.2001.0490508>
- Maia, A. Á. B., Angélica, R. S., de Freitas Neves, R., Pöllmann, H., Straub, C., & Saalwächter, K. (2014). Use of <sup>29</sup>Si and <sup>27</sup>Al MAS NMR to study thermal activation of kaolinites from Brazilian Amazon kaolin wastes. *Applied Clay Science*, *87*, 189–196. <https://doi.org/10.1016/j.CLAY.2013.10.028>
- Martina, M. C., Lorenzo, L., Giuseppe, C., Giuseppe, C., & Stefana, M. (2022). Halloysite based geopolymers filled with wax microparticles as sustainable building materials with enhanced thermo-mechanical performances. *Journal of Environmental Chemical Engineering*, *10*, 108594. <https://doi.org/10.1016/j.jece.2022.108594>
- Mbey, J. A., Thomas, F., Razafitianamaharavo, A., Caillet, C., & Villiéras, F. (2019). A comparative study of some kaolinites surface properties. *Applied Clay Science*, *172*, 135–145. <https://doi.org/10.1016/j.clay.2019.03.005>
- Medri, V., Fabbri, S., Dedeczek, J., Sobalik, Z., Tvaruzkova, Z., & Vaccari, A. (2010). Role of the morphology and the dehydroxylation of metakaolins on geopolymerization. *Applied Clay Science*, *50*, 538–545. <https://doi.org/10.1016/j.clay.2010.10.010>
- Najafi, E. K., Chenari, R. J., & Arabani, M. (2020). The potential use of clay-fly ash geopolymer in the design of active-passive liners: A review. *Clays and Clay Minerals*, *68*, 296–308. <https://doi.org/10.1007/s42860-020-00074-w>
- Nana, A., Ngouné, J., Kaze, R. C., Boubakar, L., Tchoungang, S. K., Tchakouté, H. K., Kamseu, E., & Leonelli, C. (2019). Room-temperature alkaline activation of feldspathic solid solutions: Development of high strength geopolymers. *Construction and Building Materials*, *195*, 258–268. <https://doi.org/10.1016/j.conbuildmat.2018.11.068>
- Navid, R., Carsten, K., Carsten, G., Paul, K., & Mehdi, M. (2023). Halloysite reinforced 3D-printable geopolymers. *Cement and Concrete Composites*, *136*, 104894. <https://doi.org/10.1016/j.cemconcomp.2022.104894>
- Nemaleu, J. G. D., Kaze, C. R., Tome, S., Alomayri, T., Assaedi, H., Kamseu, E., Melo, U. C., & Sglavo, V. M. (2021). Powdered banana peel in calcined halloysite replacement on the setting times and engineering properties on the geopolymer binders. *Construction and Building Materials*, *279*, 122480. <https://doi.org/10.1016/j.conbuildmat.2021.122480>
- Nicolas, S. R., Cyr, M., & Escadeillas, G. (2013). Characteristics and applications of flash metakaolins. *Applied Clay Science*, *83–84*, 253–262. <https://doi.org/10.1016/j.clay.2013.08.036>
- Nkwaju, R. Y., Djobo, J. N. Y., Nouping, J. N. F., Huisken, P. W. M., Deutou, J. G. N., & Courard, L. (2019). Iron-rich laterite-bagasse fibers based geopolymer composite: Mechanical, durability and insulating properties. *Applied Clay Science*, *183*, 105333. <https://doi.org/10.1016/j.clay.2019.105333>
- Okada, K., Ōtsuka, N., & Ossaka, J. (1986). Characterization of Spinel Phase Formed in the Kaolin-Mullite Thermal Sequence. *Journal of the American Ceramic Society*, *69*, C-251–C-253. <https://doi.org/10.1111/j.1151-2916.1986.tb07353.x>
- Parker, T. W. (1969). A Classification of Kaolinites by Infrared Spectroscopy. *Clay Minerals*, *8*, 135–141. <https://doi.org/10.1180/claymin.1969.008.2.02>
- Prasad, M. S., Reid, K. J., & Murray, H. H. (1991). Kaolin: Processing, properties and applications. *Applied Clay Science*, *6*, 87–119. [https://doi.org/10.1016/0169-1317\(91\)90001-P](https://doi.org/10.1016/0169-1317(91)90001-P)
- Provis, J. L., Lukey, G. C., & Deventer, J. S. J. (2005). Do geopolymers actually contain nanocrystalline zeolites? A reexamination of existing results. *Chemistry of Materials*, *17*, 3075–3085. <https://doi.org/10.1021/cm050230i>
- Qian, W., Feng, R., Song, S., García, R. E., Estrella, R. M., Patiño, C. L., & Zhang, Y. (2017). Geopolymerization reaction, microstructure and simulation of metakaolin-based geopolymers at extended Si/Al ratios. *Cement and Concrete Composites*, *79*, 45–52. <https://doi.org/10.1016/j.cemconcomp.2017.01.014>
- Rees, C. A., Provis, J. L., Lukey, G. C., & Deventer, J. S. J. (2007). Attenuated total reflectance fourier transform infrared analysis of fly ash geopolymer gel aging. *Langmuir*, *23*, 8170–8179. <https://doi.org/10.1021/la700713g>
- Shekhovtsova, J., Zhernovskiy, I., Kovtun, M., Kozhukhova, N., Zhernovskaya, I., & Kearsley, E. (2018). Estimation of fly ash reactivity for use in alkali-activated cements - A step towards sustainable building material and waste utilization. *Journal of Cleaner Production*, *178*, 22–33. <https://doi.org/10.1016/j.jclepro.2017.12.270>
- Singh, B. (1996). Why does halloysite roll? - A new model. *Clays and Clay Minerals*, *44*(2), 191–196. <https://doi.org/10.1346/CCMN.1996.0440204>
- Singh, P. S., Trigg, M., Burgar, I., & Bastow, T. (2005). Geopolymer formation processes at room temperature studied by <sup>29</sup>Si and <sup>27</sup>Al MAS-NMR. *Materials Science and Engineering: A*, *396*, 392–402. <https://doi.org/10.1016/j.msea.2005.02.002>
- Skibsted, J., & Andersen, M. D. (2013). The effect of alkalis on the incorporation of aluminum in the calcium

- silicate hydrate (C–S–H) phase resulting from Portland cement hydration studied by  $^{29}\text{Si}$  MAS NMR. *Journal of the American Ceramic Society*, 96, 651–656. <https://doi.org/10.1111/jace.12024>
- Smith, M. E., Neal, G., Trigg, M. B., & Drennan, J. (1993). Structural characterization of the thermal transformation of halloysite by solid state NMR. *Applied Magnetic Resonance*, 4, 157–170. <https://doi.org/10.1007/BF03162561>
- Sonuparlak, B., Sarikaya, M., & Aksay, I. A. (2005). Spinel phase formation during the 980°C exothermic reaction in the kaolinite-to-mullite reaction series. *Journal of the American Ceramic Society*, 70, 837–842. <https://doi.org/10.1111/j.1151-2916.1987.tb05637.x>
- Sun, Z., & Vollpracht, A. (2017). Isothermal calorimetry and in-situ XRD study of the NaOH activated fly ash, metakaolin and slag. *Cement and Concrete Research*, 103, 110–122. <https://doi.org/10.1016/j.cemconres.2017.10.004>
- Tan, D., Yuan, P., Annabi-Bergaya, F., Dong, F., Liu, D., & He, H. (2015). A comparative study of tubular halloysite and platy kaolinite as carriers for the loading and release of the herbicide amitrole. *Applied Clay Science*, 114, 190–196. <https://doi.org/10.1016/j.clay.2015.05.024>
- Tchakouté, H. K., Melele, S. J. K., Djamen, A. T., Kaze, C. R., Kamseu, E., Nanseu, C. N. P., Leonelli, C., & Rüschler, C. H. (2020). Microstructural and mechanical properties of poly(sialate-siloxo) networks obtained using metakaolins from kaolin and halloysite as aluminosilicate sources: A comparative study. *Applied Clay Science*, 186, 105448. <https://doi.org/10.1016/j.clay.2020.105448>
- Tian, Q., Chen, C., Wang, M., Guo, B., Zhang, H., & Sasaki, K. (2021). Effect of Si/Al molar ratio on the immobilization of selenium and arsenic oxyanions in geopolymer. *Environmental Pollution*, 274, 116509. <https://doi.org/10.1016/j.envpol.2021.116509>
- Togonovi, T. M., Petlitckaia, S., Gharzouni, A., Fricheteau, M., Texier-Mandoki, N., Bourbon, X., & Rossignol, S. (2020). High-temperature, resistant, argillite-based, alkali-activated materials with improved post-thermal treatment mechanical strength. *Clays and Clay Minerals*, 68, 211–219. <https://doi.org/10.1007/s42860-020-00067-9>
- Valentini, L. (2018). Modeling Dissolution-Precipitation Kinetics of Alkali-Activated Metakaolin. *ACS Omega*, 3, 18100–18108. <https://doi.org/10.1021/acsomega.8b02380>
- Walkley, B., & Provis, J. (2019). Solid-state nuclear magnetic resonance spectroscopy of cements. *Materials Today Advances*, 1, 100007. <https://doi.org/10.1016/j.mtadv.2019.100007>
- Wang, Y. H., Chen, J. Y., Wu, H. D., & Lei, X. R. (2017). Controllable Preparation of Zeolite P1 From Metakaolin-Based Geopolymers via a Hydrothermal Method. *Clays and Clay Minerals*, 65, 42–51. <https://doi.org/10.1346/CCMN.2016.064048>
- Wang, R., Wang, J., Dong, T., & Ouyang, G. (2020). Structural and mechanical properties of geopolymers made of aluminosilicate powder with different  $\text{SiO}_2/\text{Al}_2\text{O}_3$  ratio: Molecular dynamics simulation and microstructural experimental study. *Construction and Building Materials*, 240, 117935. <https://doi.org/10.1016/j.conbuildmat.2019.117935>
- Wang, Q., Guo, H., Yu, T., Yuan, P., Deng, L., & Zhang, B. (2022). Utilization of calcium carbide residue as solid alkali for preparing fly ash-based geopolymers: Dependence of compressive strength and microstructure on calcium carbide residue, water content and curing temperature. *Materials*, 15, 973. <https://doi.org/10.3390/ma15030973>
- Werling, N., Kaltenbach, J., Weidler, P. G., Schuhmann, R., Dehn, F., & Emmerich, K. (2022). Solubility of calcined kaolinite, montmorillonite, and illite in high molar NaOH and suitability as precursors for geopolymers. *Clays and Clay Minerals*, 70, 270–289. <https://doi.org/10.1007/s42860-022-00185-6>
- White, R. D., Bavykin, D. V., & Walsh, F. C. (2012). The stability of halloysite nanotubes in acidic and alkaline aqueous suspensions. *Nanotechnology*, 23, 065705. <https://doi.org/10.1088/0957-4484/23/6/065705>
- Yuan, P., Southon, P. D., Liu, Z. W., Green, M. E. R., Hook, J. M., Antill, S. J., & Kepert, C. J. (2008). Functionalization of halloysite clay nanotubes by grafting with gamma-aminopropyltriethoxysilane. *Journal of Physical Chemistry C*, 112, 15742–15751. <https://doi.org/10.1021/JP805657T>
- Yuan, P., Tan, D., Aannabi-Bergaya, F., Yan, W., Fan, M., Liu, D., & He, H. (2012). Changes in structure, morphology, porosity, and surface activity of mesoporous halloysite nanotubes under heating. *Clays and Clay Minerals*, 60, 561–573. <https://doi.org/10.1346/CCMN.2012.0600602>
- Yuan, P., Tan, D., & Annabi-Bergaya, F. (2015). Properties and applications of halloysite nanotubes: Recent research advances and future prospects. *Applied Clay Science*, 112–113, 75–93. <https://doi.org/10.1016/j.clay.2015.05.001>
- Yuan, J. K., He, P. G., Jia, D. C., Yang, C., Zhang, Y., Yan, S., Yang, Z. H., Duan, X. M., Wang, S. J., & Zhou, Y. (2016). Effect of curing temperature and  $\text{SiO}_2/\text{K}_2\text{O}$  molar ratio on the performance of metakaolin-based geopolymers. *Ceramics International*, 42, 16184–16190. <https://doi.org/10.1016/j.ceramint.2016.07.139>
- Yuan, P. (2016). Chapter 7 - Thermal-Treatment-Induced Deformations and Modifications of Halloysite, in: Yuan, P., Thill, A., Bergaya, F. (Eds.), *Developments in Clay Science*, 7, 137–166. <https://doi.org/10.1016/B978-0-08-100293-3.00007-8>
- Zhang, Z. H., Xiao, Y., Huajun, Z., & Yue, C. (2009). Role of water in the synthesis of calcined kaolin-based geopolymer. *Applied Clay Science*, 43, 218–223. <https://doi.org/10.1016/j.clay.2008.09.003>
- Zhang, Z., Wang, H., Yao, X., & Zhu, Y. (2012a). Effects of halloysite in kaolin on the formation and properties of geopolymers. *Cement and Concrete Composites*, 34, 709–715. <https://doi.org/10.1016/j.cemconcomp.2012.02.003>
- Zhang, Z. H., Wang, H., Provis, J. L., Bullen, F., Reid, A., & Zhu, Y. C. (2012b). Quantitative kinetic and structural analysis of geopolymers. Part 1. The activation of metakaolin with sodium hydroxide. *Thermochimica Acta*, 539, 23–33. <https://doi.org/10.1016/j.tca.2012.03.021>
- Zhang, Z. H., Provis, J. L., Wang, H., Bullen, F., & Reid, A. (2013). Quantitative kinetic and structural analysis of geopolymers. Part 2. Thermodynamics of sodium silicate activation of metakaolin. *Thermochimica Acta*, 565, 163–171. <https://doi.org/10.1016/j.tca.2013.01.040>
- Zhang, Z. H., Zhu, H. J., Zhou, C. H., & Wang, H. (2016). Geopolymer from kaolin in China: An overview. *Applied Clay Science*, 119, 31–41. <https://doi.org/10.1016/j.clay.2015.04.023>

- Zhang, B., Guo, H., Deng, L., Fan, W., Yu, T., & Wang, Q. (2020a). Undehydrated kaolinite as materials for the preparation of geopolymer through phosphoric acid-activation. *Applied Clay Science*, *199*, 105887. <https://doi.org/10.1016/j.clay.2020.105887>
- Zhang, B., Guo, H., Yuan, P., Li, Y., Wang, Q., Deng, L., & Liu, D. (2020b). Geopolymerization of halloysite via alkali-activation: Dependence of microstructures on precalcination. *Applied Clay Science*, *185*, 105375. <https://doi.org/10.1016/j.clay.2019.105375>
- Zhang, B., Guo, H., Yuan, P., Deng, L., & Liu, D. (2020c). Novel acid-based geopolymer synthesized from nanosized tubular halloysite: The role of precalcination temperature and phosphoric acid concentration. *Cement and Concrete Composites*, *110*, 103601. <https://doi.org/10.1016/j.cemconcomp.2020.103601>
- Zhang, B., Yuan, P., Guo, H., Deng, L., Li, Y., Li, L., Wang, Q., & Liu, D. (2021). Effect of curing conditions on the microstructure and mechanical performance of geopolymers derived from nanosized tubular halloysite. *Construction and Building Materials*, *268*, 121186. <https://doi.org/10.1016/j.conbuildmat.2020.121186>
- Zhang, B., Yu, T., Deng, L., Li, Y., Guo, H., Zhou, J., Li, L., & Yuan, P. (2022). Ion-adsorption type rare earth tailings for preparation of alkali-based geopolymer with capacity for heavy metals immobilization. *Cement and Concrete Composites*, *134*, 104768. <https://doi.org/10.1016/j.cemconcomp.2022.104768>

Springer Nature or its licensor (e.g. a society or other partner) holds exclusive rights to this article under a publishing agreement with the author(s) or other rightsholder(s); author self-archiving of the accepted manuscript version of this article is solely governed by the terms of such publishing agreement and applicable law.